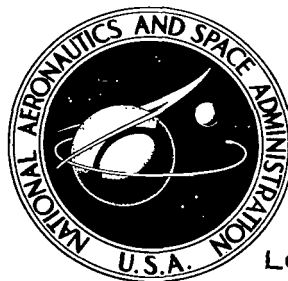


**NASA TECHNICAL NOTE**



**NASA TN D-8400** *c.1*

**NASA TN D-8400**

LOAN COPY: RE  
AFWL TECHNICAL  
KIRTLAND AFB



**AERODYNAMIC HEATING IN LARGE CAVITIES  
IN AN ARRAY OF RSI TILES**

*L. Roane Hunt*

*Langley Research Center*

*Hampton, Va. 23665*



0134125

1. Report No. NASA TN D-8400		2. Government Accession No.		3. Recipient's Catalog No.	
4. Title and Subtitle AERODYNAMIC HEATING IN LARGE CAVITIES IN AN ARRAY OF RSI TILES		5. Report Date May 1977		6. Performing Organization Code	
		8. Performing Organization Report No. L-11221		10. Work Unit No. 506-17-22-01	
7. Author(s) L. Roane Hunt		9. Performing Organization Name and Address NASA Langley Research Center Hampton, VA 23665		11. Contract or Grant No.	
12. Sponsoring Agency Name and Address National Aeronautics and Space Administration Washington, DC 20546		13. Type of Report and Period Covered Technical Note		14. Sponsoring Agency Code	
		15. Supplementary Notes			
16. Abstract <p>A large panel of reusable surface insulation (RSI) tiles including lost-tile cavities was aerothermally tested in the Langley 8-foot high-temperature structures tunnel to determine both the heat load within the cavities and the structural performance of the RSI surrounding the cavities. Tests were conducted with a turbulent boundary layer at a nominal free-stream Mach number of 6.6, a total temperature of 1800 K, a Reynolds number per meter of <math>5 \times 10^6</math>, and a dynamic pressure of 62 kPa. The maximum aerodynamic heating to the floor of the cavity was two to three times the normal surface heating. The cavity heating rates agreed with data from other facilities and were successfully correlated with an empirical equation. A zippering failure occurred to a tile downstream of a double-tile cavity when the separated flow attached to the floor of the cavity and forced the tile from its position.</p>					
17. Key Words (Suggested by Author(s)) Aerodynamic heating Cavities Surface insulation Thermal protection			18. Distribution Statement Unclassified - Unlimited  Subject Category 34		
19. Security Classif. (of this report) Unclassified	20. Security Classif. (of this page) Unclassified	21. No. of Pages 36	22. Price* \$4.00		

# AERODYNAMIC HEATING IN LARGE CAVITIES

## IN AN ARRAY OF RSI TILES

L. Roane Hunt  
Langley Research Center

### SUMMARY

A large panel of reusable surface insulation (RSI) tiles including lost-tile cavities was aerothermally tested in the Langley 8-foot high-temperature structures tunnel to determine both the heat load within the cavities and the structural performance of the RSI surrounding the cavities. Tests were conducted with a turbulent boundary layer at a nominal free-stream Mach number of 6.6, a total temperature of 1800 K, a Reynolds number per meter of  $5 \times 10^6$ , and a dynamic pressure of 62 kPa. The maximum aerodynamic heating to the floor of the cavity was two to three times the normal surface heating. The cavity heating rates agreed with data from other facilities and were successfully correlated with an empirical equation. A zippering failure occurred to a tile downstream of a double-tile cavity when the separated flow attached to the floor of the cavity and forced the tile from its position.

### INTRODUCTION

The thermal protection system (TPS) for the space shuttle consists of reusable surface insulation (RSI) tiles bonded to the exterior of the primary structure (refs. 1, 2, and 3). The RSI is a ceramic material consisting of rigidized, silica-fiber insulation with a borosilicate coating and designated LI-942. If any of these tiles debond prior to entry into the atmosphere, the primary structure will be exposed to the hot boundary-layer gases associated with entry. Tiles may be shaken loose during ascent when vibration due to engine noise is most severe, or they may be damaged in orbit by the impact of orbiting debris or near field experiments. In either case, lost (or missing) tiles would produce large surface cavities which would, in turn, expose the primary structure to aerothermal effects which must be investigated. Existing experimental heating-rate data (ref. 4 and unpublished data taken in the Ames 20 MW Semi-Elliptical Duct) are limited to small models and cavities representative of only single lost tiles. Additional heating-rate data for a broader range of cavity dimensions in larger tile arrays are required to evaluate the integrity of the tile system in the event of tile losses.

Consequently, aerothermal tests were made by using an existing TPS panel (ref. 5) modified to simulate single and double lost-tile cavities in a shuttle RSI tile array. The tests were conducted in the Langley 8-foot high-temperature structures tunnel where the free-stream Mach number was 6.6, the total temperature was 1800 K, the Reynolds number per meter was  $5 \times 10^6$ , and the dynamic pressure was 62 kPa. The model was tested at angles of attack of  $0^\circ$  and  $15^\circ$

with turbulent-boundary-layer and surface shear-stress values of 56 and 230 Pa, respectively.

This paper presents both the experimental heating-rate distribution within lost-tile cavities and the calculated thermal response of a primary structure that was exposed within a lost-tile cavity during shuttle entry. The structural integrity of tiles surrounding cavities is also indicated.

Commercial products are used in this report to adequately describe the model. These commercial products do not constitute official endorsement, expressed or implied, of such products or manufacturers by the National Aeronautics and Space Administration.

#### SYMBOLS

$d, l, w$	cavity dimensions (see fig. 4), m
$M$	Mach number
$p$	pressure, Pa
$Q$	normalized heating-rate distribution (eq. (A1))
$q$	dynamic pressure, Pa
$\dot{q}$	heating rate, $W/m^2$
$\dot{q}_{fp}$	flat-plate heating rate, $W/m^2$
$R$	Reynolds number per meter
$s$	wetted distance along cavity perimeter from reattachment corner (see fig. 8), m
$T$	temperature, K
$\Delta T$	temperature increase during aerothermal testing, K
$t$	time, s
$\Delta t$	aerothermal testing time, s
$x$	distance in flow direction (see fig. 4), m
$\bar{x}$	normalized distance, $1 - (x/l)$
$\alpha$	angle of attack, deg
$\delta^*$	boundary-layer displacement thickness, m
$\tau$	local flow shear stress, Pa

## Subscripts:

aw	adiabatic wall condition
l	local condition
t	total condition
w	wall condition
$\infty$	free-stream condition

## APPARATUS AND TEST

### Model Description

The lost-tile cavity tests were conducted by using an existing TPS panel mounted in the facility panel holder. (See fig. 1.) The panel is constructed of external insulation tiles bonded to a strain isolator which is, in turn, bonded to the primary structure. The basic panel is 91.4 by 137.2 cm and consists of 22.9- by 22.9- by 3.24-cm mullite tiles and a 0.76-cm-thick, silicone-foam strain isolator (PD-200). Mullite is made of fibers from a mixture of oxides (77 percent alumina) rigidized by an alumina-boria-silica binder. The primary structure was fabricated from 0.1-cm-thick sheets of titanium. This panel design was an early candidate for the space shuttle and is described in more detail in reference 5.

Single and double lost-tile cavities were formed in the tile array by removing portions of the tiles from the basic panel. The cavity dimensions and the surface condition of the cavity floor prior to each test are summarized in table I. The single-tile cavity A is bordered by the mullite tiles of the basic panel and the cavity floor (or primary structure) is covered by a 0.32-cm-thick Nomex felt strain isolator pad (SIP) with a silicone rubber (RTV 560) bond similar to the SIP used on the shuttle. The single-tile cavity B is bounded on three sides by the mullite tiles and on the downstream side by two space shuttle RSI (LI-942) tiles. The RSI tiles (14.2 by 14.2 by 3.8 cm) and the Nomex SIP are bonded to the primary structure. The floor of cavity B is bare. Cavity A was subjected to all four tests; cavity B was subjected to tests 1 and 2 only.

After test 2 for cavity B, the first downstream tile of the cavity was removed to produce the double-tile cavity shown in table I; this cavity, with the primary-structure skin bare, was designated cavity C and was subjected to test 3. For test 4, one-half the width of the cavity floor was covered by SIP between two layers of RTV bond; this was designated cavity D. Photographs of the single- and double-tile cavity configurations are shown in figures 2 and 3.

### Model Instrumentation

Thermocouples were installed beneath the cavities to determine the heating-rate distribution to the cavity floor. These thermocouples were located on the

back side of spot welds where the structural skin was attached to the stiffeners. The thermocouple (TC) locations are indicated in figure 4. The shaded portion of the cavities in figure 4(c) is the area that was covered with SIP (designated cavity D). Also, thermocouples were embedded in the top surface coating of the tiles and were attached to the primary structure beneath the tiles upstream of the cavities.

### Facility

The tests were conducted in the Langley 8-foot high-temperature structures tunnel, which is shown schematically in figure 5. This facility is a hypersonic blowdown wind tunnel that uses the combustion products of methane and air as the test medium and operates at a nominal Mach number of 7, at total pressures between 3.4 and 24.1 MPa, and at nominal total temperatures between 1400 K and 2000 K. Corresponding free-stream Reynolds numbers per meter are between  $1 \times 10^6$  and  $10 \times 10^6$ . These conditions simulate the aerothermal flight environment at Mach 7 in the altitude range between 25 and 40 km. The panel holder (fig. 1) is retained in the pod below the test chamber during facility startup and shutdown and is covered by acoustic baffles which protect the panel from the potentially damaging acoustic disturbance and buffeting that are generated during facility startup and shutdown. The model is inserted when the desired stream conditions are established. Although the facility provides aerodynamic exposure times of up to 120 s, thermal exposure times can be extended indefinitely by means of a pair of retractable quartz-lamp radiant heaters located in the pod. Additional information pertaining to this equipment and to the test facility may be found in references 6 and 7.

### Test Procedure

Prior to the aerodynamic exposure, the test panel was heated by radiant lamps in the pod of the tunnel to represent the initial thermal profile of a typical shuttle entry. When the desired temperature was reached, the lamps were retracted and the model was rapidly inserted into the test stream for 8 to 25 s. During the radiant heat phase, the lost-tile cavities were filled by pillows made of fibrous silica insulation and were covered by a cloth of woven silica fibers to prevent heating of the primary structure. (See fig. 6(a).) As the radiant heaters were retracted, the pillows were removed from the cavities by pull ribbons attached to the heater covers. (See fig. 6(b).) A photograph of typical cavity pillows and a pull ribbon is shown in figure 7. The intent of this procedure was to simulate a tile loss during entry when the upstream tile surface was hot and the primary structure was cold.

### Tests

Four wind-tunnel tests were made on the various lost-tile cavity configurations. The surface conditions of the cavity floors are summarized in table I. The test sequence and test conditions are listed in table II. The conditions include exposure times, delay time, maximum surface temperatures, flat-plate heating levels to the tile surfaces, and angle of attack. (The delay time is

the interval between the end of radiant heating and the beginning of aerodynamic heating.) The flat-plate heating rate was obtained from the calibration tests of reference 7. The free-stream and local aerodynamic flow conditions for each test are listed in table III. The calculated boundary-layer displacement thickness and surface shear stress at the cavities are given in table III, but a more detailed description of the turbulent boundary layer is given in reference 8.

## RESULTS AND DISCUSSION

### Summary of Test Results

The absence of one or more tiles from the RSI tile array considered in this investigation produced a rectangular cavity with predominately two-dimensional cavity flow. As described in reference 4, there are two stable cavity-flow conditions which can exist for supersonic flow. One flow condition, illustrated in figure 8(a), is designated "open cavity flow," where the length-to-depth ratio  $l/d$  is less than about 10. The flow spans the cavity and reattaches to the top of the downstream wall at point C. A free shear layer B exists between the external flow and the circulating separated flow D. The other flow condition (fig. 8(b)) is designated "closed cavity flow," where the length-to-depth ratio is greater than about 14. The flow expands into the cavity and reattaches to the floor, flows along the floor, and separates ahead of the downstream wall. Both the single- and double-tile cavities tested herein had  $l/d$  values less than 10, which indicated that open cavity flow should exist.

The posttest condition of each of the lost-tile cavity configurations is shown in figure 9. After test 1, the downstream one-third of the SIP of cavity A was charred although no visible degradation had occurred to cavity B or to tiles 1 and 2. After test 2, the SIP in cavity A was completely charred, and the upstream surface of tile 1 was chipped on the upper edge by foreign particle impact. No appreciable damage occurred during test 3. During test 4, the downstream wall of cavity A was damaged by foreign particle impact. Considerable damage occurred in cavity D as follows: first the forward edge of tile 2 eroded. Then the flow attached to the floor (fig. 8(b)) and dislodged tile 2. The mullite tile behind tile 2 then eroded until the model was retracted from the stream. This behavior is discussed in more detail later.

### Aerothermal Response of Bare Cavity Floor

Typical thermal response of the test model is shown in figure 10. The temperature histories at the locations indicated by the inset are presented for both the radiant-heating and aerodynamic-heating phases of test 2. During radiant heating, the tile surface (location ①) was heated to 1180 K and was held at this temperature for 450 s. At  $t = 828$  s, the radiant heaters were retracted to uncover the cavities. The model was then inserted into the test stream for an exposure of 8 s. The time scale from 828 to 850 s is expanded to show more detail. The temperature histories at locations ③ and ④ on the floor of cavity B are compared with that at location ② under a tile. The highest thermal response occurred at location ③ at the base of the downstream wall of the cavity.

## Aerodynamic Heating Distribution Along Cavity Floors

The temperature distributions along the cavity floors after the radiant preheat and before the aerodynamic exposure are presented in figure 11. Figure 11(a) is for tests 1 and 2 of cavity B; figure 11(b) is for tests 3 and 4 of cavities C and D, respectively. The temperatures at the cavity ends were higher than the middle because of radiant-heat penetration between the pillows and the tiles. (See fig. 11(b), test 4.) These temperature variations existed when heating rates were evaluated. Therefore, the cavity heating rates were converted to cold-wall heating rates by multiplying them by the ratio  $(T_{aw} - 300)/(T_{aw} - T_w)$ , where the cold-wall reference temperature is 300 K.

The ratio of the cavity heating rate to the local flat-plate heating rate is plotted as a function of longitudinal distance along the cavity floor in figure 12. For single- and double-tile cavities, the maximum cavity heating at the base of the downstream wall of the cavity was about two and three times the local flat-plate value, respectively. The cavity heating decreased monotonically along the cavity floor from the downstream wall.

The normalized heating rates for all the present tests are correlated in figure 13 where they are plotted against the normalized distance along the cavity floor  $\bar{x}$ , defined as the quantity  $1 - (x/l)$ . The present data are plotted as the solid symbols and are compared with two other sets of data obtained from reference 4 and from the Ames 20 MW Semi-Elliptical Duct (unpublished). The data represented by the open circular symbols were obtained from reference 4 for a rectangular cavity with a length-to-depth ratio of 5. These data were obtained in the AEDC Tunnel C for a local Mach number of 6.3 and a total temperature of 1050 K. The data represented by the open square symbols were obtained in the Ames 20 MW Semi-Elliptical Duct where the cavity was skewed 45° to the flow as shown by the insert in figure 13. These data were obtained for a Mach number of about 5. Good agreement in the heating rates was obtained in this correlation for the two different cavity orientations and the wide variations in cavity geometry. The largest variation in the data is between  $\bar{x} = 0.3$  and 0.7. The origin of  $\bar{x}$  was chosen to coincide with the location of a secondary flow reattachment which probably existed at the base of the downstream wall of these cavities. This flow reattachment, indicated by increased pressure and heating rates at that location, was evident in the experimental results for the shallow cavities of references 4 and 9. The dashed-line curve in figure 13 is represented by the equation

$$\frac{\dot{q}}{\dot{q}_{fp}} = 0.27(\bar{x})^{-0.74} \quad (1)$$

which is similar to that suggested in reference 10 for the decay of heating rate with distance from the impingement of a turbulent free-jet flow. As can be seen, the data along the cavity floor are correlated very well by this empirical equation.

The heating-rate distributions shown by the solid curves in figure 13 are based on the theoretical model of reference 11 which accounts for energy transferred across a free shear layer (fig. 8) of deep open cavities. Curves are



shown for both laminar and turbulent flows, and the forms of the equations used are given in the appendix. The theory assumes an inviscid rotational flow within the cavity with an inherent monotonic decay in heating rate along the wetted surfaces of the cavity from the flow reattachment corner to the flow separation corner. (See fig. 8(a).) However, as noted previously, references 4 and 9 identified a secondary flow reattachment at the base of the downstream wall ( $\bar{x} \approx 0$ ) which produced increased heating rates. Also, reference 8 has shown that, for small open cavities, heating rates on the upstream wall increase, rather than decrease, from the base to the flow separation corner. The theoretical curves bracket the experimental data over most of the cavity floor, but the high heating rates at  $\bar{x} = 0.03$  may have been caused by the secondary flow reattachment. The theoretical model is probably inadequate to define the detail heating-rate distribution for the open cavity dimensions herein; however, it has been applied successfully in reference 12 for the downstream wall and floor of deep cavities.

#### Thermal Response of Structural Skin Covered by SIP

The single-tile cavities A and B differed in that the floor of cavity A was covered by the Nomex SIP material and the floor of cavity B was bare. As indicated in figure 4(a), only one thermocouple was attached to the structure beneath cavity A. In figure 14 the temperature responses of this thermocouple (location ①) for each test and for both angles of attack are compared with the response of a corresponding thermocouple in cavity B (location ②) where the skin was bare. The results for tests 1 and 2 when the Nomex was uncharred indicate that the SIP insulated the skin substantially, but only for a short time. The thermal protection decreased when the Nomex SIP charred, as shown by the results of tests 3 and 4. These results indicate that SIP alone does not offer extended thermal protection for the primary structure.

A similar comparison is made in figure 15 on the double-tile cavity in test 4 where the floor of the cavity was divided into two equal longitudinal strips: one bare and the other covered with Nomex SIP sandwiched between layers of RTV 560. The change in temperature of the floor is plotted against the test time where the model was inserted into the stream at about 509 s. The temperature rise rate of the bare floor at location ⑥ increased sharply at about  $t = 514.4$  s; this suggests a change in flow characteristics from open to closed cavity flow with the separated flow attaching to the floor of the cavity. (See fig. 8.) In fact, location ② experienced a temperature rise (or burnthrough of the SIP) sooner than locations ① or ③; this indicated that the reattachment to the floor was closer to location ②. The front edge of tile 2 had eroded until the effective  $l/d$  was great enough to allow closed cavity flow. At  $t = 515.36$  s tile 2 was forced from its position, as indicated by the photographic data. After burnthrough, locations ① and ② experienced a temperature rise rate equal to that of location ⑥. Locations ③ and ④ experienced some temperature rise prior to model retraction from the stream. Posttest inspection indicated that the SIP at location ⑤ was intact. In the present test, the SIP is shown to provide some temporary thermal protection within the cavity unless the heating load is great enough to cause burnthrough.

## Tile Failure by Zippering

The term "zippering" refers to a potential catastrophic failure of the RSI tile system where tiles sequentially peel off as their bond lines are exposed by the departure of upstream tiles. In the present tests, zippering occurred only for the most severe test condition with a double lost-tile cavity. The zippering failure is shown in figure 16 by the sequence of photographs from test 4. These photographs are taken from behind the model looking upstream; cavities A and D are indicated. At  $t = 510$  s, the front edge of tile 2 has begun to erode. Between  $t = 510$  and  $515.36$  s, the front edge of tile 2 continued to erode until most of the top surface of tile 2 was removed. Increased erosion occurred near each of the upstream corners of the tile. As the tile eroded, the effective cavity length-to-depth ratio  $l/d$  increased; apparently, the separated flow attached to the floor of the cavity and the remaining two-thirds of tile 2 was dislodged at  $t = 515.36$  s. The remaining photographs show the erosion of the mullite tile before the model was retracted from the stream. Zippering probably would have continued if the downstream mullite tile had been attached to the structural skin with Nomex SIP instead of silicone foam.

Photographs of the damaged area after test 4 are presented in figure 17. Most of the Nomex SIP beneath tile 2 was burned away and left only part of the base layer of RTV bond. The mullite tile behind the cavity was severely eroded, but it does not appear to have been in danger of zippering. The silicone foam beneath the mullite tile eroded at about the same rate as the tile. The Nomex SIP under the LI-942 tiles is a low-temperature material and will burn beneath the tiles if it is exposed to the hot gases associated with entry. For example, about 2 cm of Nomex beneath tile 1 was burned during tests 1 and 2, as indicated when tile 1 was removed after test 2. In test 4, the Nomex SIP under tile 2 probably burned so badly that the bond could not be maintained. Thus, it appears that if separated flow does attach to the cavity floor (closed cavity flow), low-temperature bond-line material will burn to produce the zippering failure.

The aerodynamic heating-rate distribution in cavity D during test 4 is presented in figure 18. The heating rate to the bare skin is compared with that of the skin covered with SIP before and after tile 2 was blown clear. At  $t = 510.2$  s (before zippering), the heating distribution on the bare skin is the same as that presented in figure 12(b). The corresponding heating to the skin covered with SIP is essentially zero. After tile 2 is gone at  $t = 517.5$  s, the flow attaches to the cavity floor and the heating over most of the instrumented area of the bare skin was equivalent to the flat-plate value. In the area where the SIP burned through, the heating level was also at the flat-plate value.

### Effect of Cavity Heating on Vehicle Structure

The thermal response of a structure exposed in a single lost-tile cavity during shuttle entry was computed by using the present heating-rate correlation and is presented in figure 19. The locations for which temperature histories were computed are given in the inset. The temperatures for the tile surface (location ①) and the structure beneath the tile (location ②) are represented

by the solid curves. These temperatures were determined from a one-dimensional thermal analysis of a 3.81-cm-thick tile exposed to the shuttle entry heating of reference 13 with a maximum heating rate of 88.6 kW/m<sup>2</sup>. The analytical heat balance of the structure at location ③ is also indicated in the inset. The aluminum structure is represented by a single sheet 0.2 cm thick. The aerodynamic heating to the exposed structure was determined by multiplying the cavity normalized heating-rate values of equation (1) by the heating-rate history of reference 13. Heat was assumed to be conducted along the structure but not into the insulation beneath the structure or into the adjacent tiles. The predetermined temperature history at location ② (8 tiles, or 114 cm, downstream) was assumed to be the boundary condition in computing the temperature response at location ③. Location ② was far enough away from the cavity to be unaffected by the increased heating of the structure at the cavity. Three temperature histories (dashed-line curves) were computed for the structure at location ③ where the tile was assumed to have been lost at various times during entry. The lost tile at 500 s corresponds to the time of maximum heating. These results indicate that, for the region of the shuttle vehicle where the tile is 3.81 cm thick with a maximum surface temperature of 1170 K, the aluminum primary structure would melt if a tile were lost within the first 1000 s of entry.

#### CONCLUDING REMARKS

A thermal protection system panel 91.4 cm by 137.2 cm consisting of reusable surface insulation (RSI) tiles bonded to a primary structure was modified to include single and double lost-tile cavities. This panel was subjected to four aerothermal tests in the Langley 8-foot high-temperature structures tunnel to determine both the aerodynamic heat load within the cavities and the structural performance of the RSI surrounding the cavities. Tests were conducted with a turbulent boundary layer at a nominal free-stream Mach number of 6.6, a total temperature of 1800 K, a Reynolds number per meter of  $5 \times 10^6$ , and a dynamic pressure of 62 kPa.

The maximum aerodynamic heating to the floor of the cavity was two or three times the normal surface heating. The cavity heating rates agreed with other data for cavities of various sizes and flow orientations and were successfully correlated with an empirical equation. Calculated structure temperature for a 3.81-cm-deep single-tile cavity exposed to simulated shuttle entry conditions indicated that the aluminum structural skin would melt if the tile were lost within the first 1000 s of entry. The strain isolator pad (SIP) does not offer extended thermal protection to the structure when a tile is lost. A zippering failure occurred to the tile downstream of the double lost-tile cavity when the separated flow attached to the floor of the cavity. The attached flow ablated the SIP beneath the tile and forced the tile from its position.

Langley Research Center  
National Aeronautics and Space Administration  
Hampton, VA 23665  
February 28, 1977

## APPENDIX

### THEORETICAL HEATING-RATE DISTRIBUTION

The analytical approach for the present shallow cavities uses the theory of reference 11 and follows an approach similar to that suggested in reference 12 for deep rectangular cavities. In reference 11, the flow was modeled as an inviscid rotational core with uniform vorticity and uniform total enthalpy separated from the external flow by a recirculating viscous layer (or a viscous free shear layer). The equations governing the flow in a square cavity (single recirculating eddy) were determined and then extended by an approximate linearized method to include deep rectangular cavities. The linearized results were compared with numerical solutions of the full Navier-Stokes equations and were found to be in good agreement.

The linearized solution of the momentum equations was extended in reference 11 to solve the energy equation which was further simplified by assuming a Prandtl number of 1. A normalized heating-rate distribution  $Q$  is defined as the ratio of the local heating rate on the surface of a finite-depth cavity to the average heating rate across the separation streamline for an infinitely deep cavity. The equation for the normalized heating-rate distribution developed in reference 11 is

$$Q = \frac{1}{2\sqrt{2\left(1 + \frac{d}{l}\right)}} \left\{ \zeta\left[\frac{1}{2}, \frac{s}{2(l+d)}\right] - \zeta\left[\frac{1}{2}, \frac{s+l}{2(l+d)}\right] \right\} \quad (A1)$$

where  $d$ ,  $l$ , and  $s$  are defined in figure 8 and  $\zeta(u, v)$  is the generalized Riemann zeta function. The function  $\zeta\left(\frac{1}{2}, v\right)$  has been tabulated in reference 14 and is given to an accuracy of one part in 100 000 by the following curve-fit equation (from ref. 11):

$$\zeta\left(\frac{1}{2}, v\right) = \frac{1}{\sqrt{v}} + \sum_{n=0}^5 a_n (v+1)^n \quad (0 < v < 1) \quad (A2)$$

where the coefficients  $a_n$  are

$$a_0 = 0.803323$$

$$a_1 = -3.89728$$

$$a_2 = 2.55002$$

$$a_3 = -1.19121$$

APPENDIX

$$a_4 = 0.308284$$

$$a_5 = -0.0335024$$

In reference 11,  $\dot{q}/\dot{q}_{fp}$  is obtained by multiplying  $Q$  by the percentage of energy transferred into the cavity through the free shear layer produced by flow separation. For laminar flow, reference 15 shows that about 60 percent of the energy is transferred into the cavity. Thus, the cavity heating-rate is given by the following equation:

(Laminar)

$$\frac{\dot{q}}{\dot{q}_{fp}} = 0.6Q = \frac{0.21}{\sqrt{1 + \frac{d}{l}}} \left\{ \zeta \left[ \frac{1}{2}, \frac{s}{2(1+d)} \right] - \zeta \left[ \frac{1}{2}, \frac{s+l}{2(1+d)} \right] \right\} \quad (A3)$$

For turbulent flow, reference 16 shows that the energy transferred into the cavity is about 3.5 times the normal surface heating. Thus, the cavity heating-rate distribution is given by the following equation:

(Turbulent)

$$\frac{\dot{q}}{\dot{q}_{fp}} = 3.5Q = \frac{1.24}{\sqrt{1 + \frac{d}{l}}} \left\{ \zeta \left[ \frac{1}{2}, \frac{s}{2(1+d)} \right] - \zeta \left[ \frac{1}{2}, \frac{s+l}{2(1+d)} \right] \right\} \quad (A4)$$

Equations (A3) and (A4) are plotted in figure 13 for a value of  $l/d = 6$ .

## REFERENCES

1. Anderson, Roger A.; Brooks, William A., Jr.; Leonard, Robert W.; and Maltz, Joseph: Structures - A Technology Overview. Astronaut. & Aeronaut., vol. 9, no. 2, Feb. 1971, pp. 38-47.
2. Love, Eugene S.: Advanced Technology and the Space Shuttle. Astronaut. & Aeronaut., vol. 11, no. 2, Feb. 1973, pp. 30-66.
3. Strouhal, George; and Tillian, Donald J.: Testing the Shuttle Heat-Protection Armor. Astronaut. & Aeronaut., vol. 14, no. 1, Jan. 1976, pp. 57-65.
4. Nestler, D. E.; Saydah, A. R.; and Auxer, W. L.: Heat Transfer to Steps and Cavities in Hypersonic Turbulent Flow. AIAA Paper No. 68-673, June 1968.
5. Hunt, L. Roane: Performance of a Mullite Reusable Surface Insulation System in a Hypersonic Stream. NASA TM X-3397, 1976.
6. Deveikis, William D.; Bruce, Walter E., Jr.; and Karns, John R.: Techniques for Aerothermal Tests of Large, Flightweight Thermal Protection Panels in a Mach 7 Wind Tunnel. NASA TM X-71983, 1974.
7. Deveikis, William D.; and Hunt, L. Roane: Loading and Heating of a Large Flat Plate at Mach 7 in the Langley 8-Foot High-Temperature Structures Tunnel. NASA TN D-7275, 1973.
8. Weinstein, Irving; Avery, Don E.; and Chapman, Andrew J.: Aerodynamic Heating to the Gaps and Surfaces of Simulated Reusable-Surface-Insulation Tile Arrays in Turbulent Flow at Mach 6.6. NASA TM X-3225, 1975.
9. McDearmon, Russell W.: Investigation of the Flow in a Rectangular Cavity in a Flat Plate at a Mach Number of 3.55. NASA TN D-523, 1960.
10. Nestler, D. E.: An Engineering Analysis of Reattaching Shear Layer Heat Transfer. AIAA Paper No. 72-717, June 1972.
11. Burggraf, Odus R.: A Model of Steady Separated Flow in Rectangular Cavities at High Reynolds Number. Proceedings of the 1965 Heat Transfer and Fluid Mechanics Institute, Andrew F. Charwat, ed., Stanford Univ. Press, 1965, pp. 190-229.
12. Wieting, Allan R.: Experimental Investigation of Heat-Transfer Distributions in Deep Cavities in Hypersonic Separated Flow. NASA TN D-5908, 1970.
13. Ebbesmeyer, L. H.; and Christensen, H. E.: Silica Heat Shield Sizing. Rep. MDC E1343. (Contract NAS2-7897) McDonnell Douglas Corp., July 24, 1975. (Available as NASA CR-151962.)

14. Powell, E. O.: A Table of the Generalized Riemann Zeta Function in a Particular Case. Quart. J. Mech. Appl. Math., vol. V, Pt. 1, Mar. 1952, pp. 116-123.
15. Chapman, Dean R.: A Theoretical Analysis of Heat Transfer in Regions of Separated Flow. NACA TN 3792, 1956.
16. Gray, K. Evan; Ruhmel, Dale B.; and Donaldson, Coleman duP.: A Simplified Study of the Turbulent Free Shear Layer Between Two Dissimilar Gases. Rep. No. 72, Aeronaut. Res. Assoc. Princeton, Inc., July 1965.

TABLE I.- LOST-TILE CAVITY CONFIGURATIONS AND PRETEST CONDITIONS

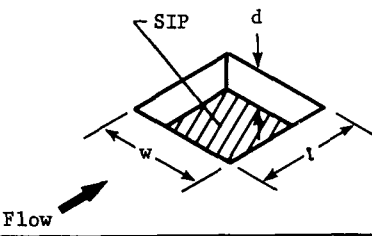
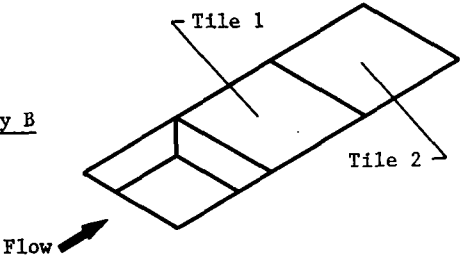
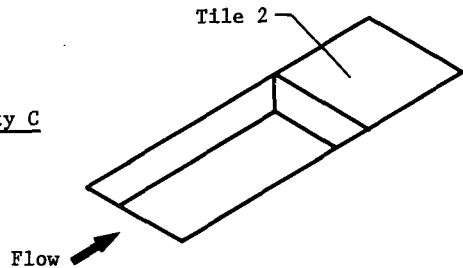
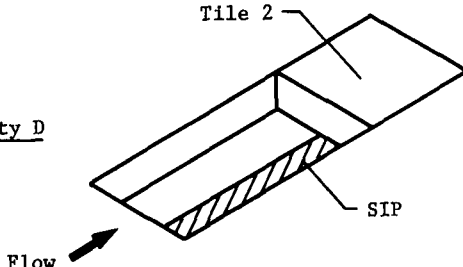
Configuration	d, cm	l, cm	w, cm	Test	Surface condition of cavity floor
<u>Cavity A</u> 	4.1	15.0	14.2	1	Nomex/RTV bond
				2	Partially charred Nomex/RTV bond
				3	Charred Nomex/RTV bond
				4	Charred Nomex/RTV bond
<u>Cavity B</u> 	4.1	16.8	14.7	1	Bare
				2	Bare
<u>Cavity C</u> 	4.1	31.5	14.7	3	Bare
<u>Cavity D</u> 	4.1	31.5	14.7	4	One-half bare, the other half covered with RTV bond/Nomex/RTV bond



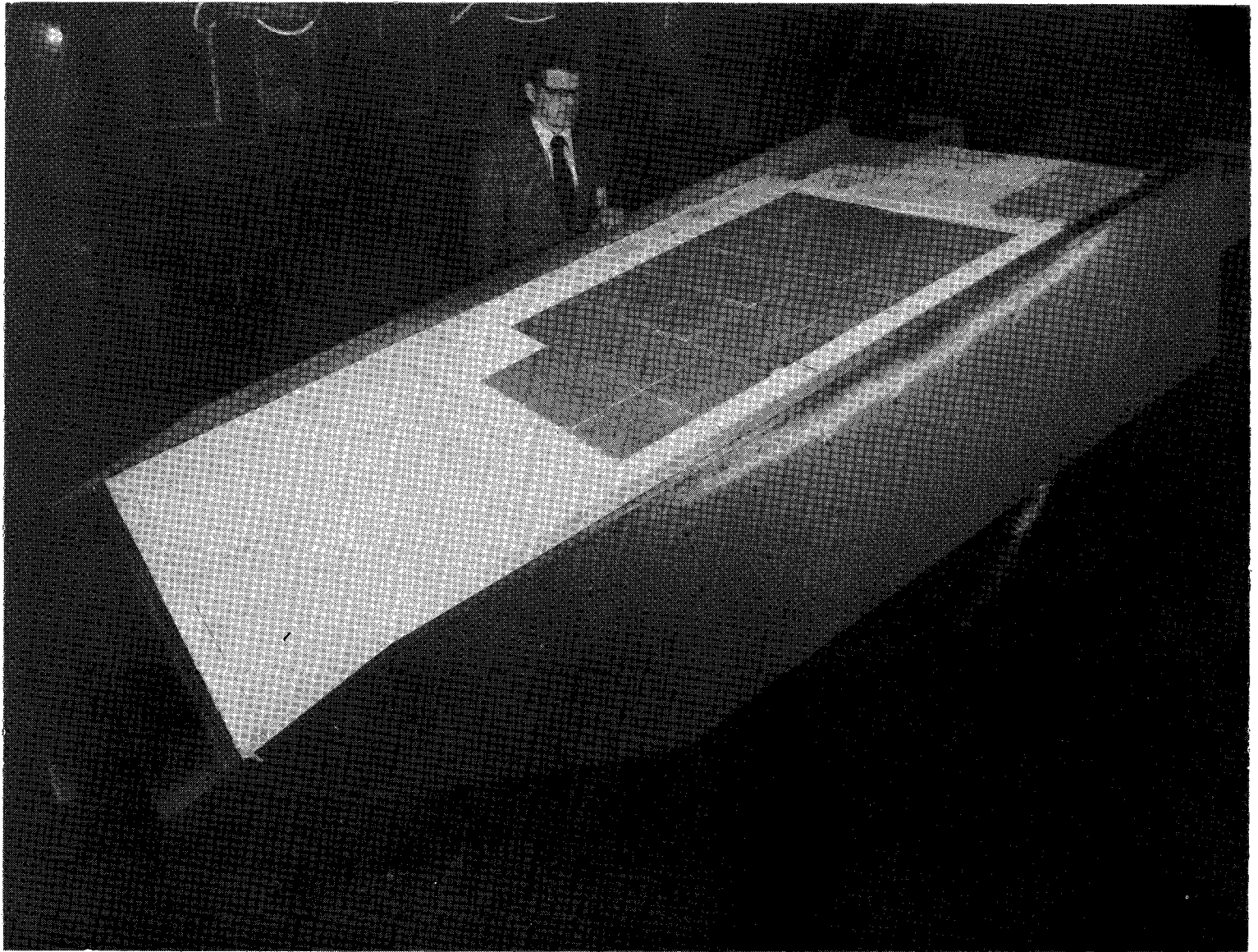
TABLE II.- TEST SEQUENCE AND EXPOSURE TIMES

Test	Radiant heating			Delay time, s (a)	Aerodynamic heating			
	Heatup time, s	Time at maximum surface temperature, s	Maximum surface temperature, K		Time in stream, s	Surface temperature in stream, K	$\dot{q}_{fp}$ , kW/m <sup>2</sup>	$\alpha$ , deg
1	230	430	960	6	10	920	51.7	0
2	380	450	1180	10	8	1200	251	15
3	270	190	1000	5	25	1000	66.3	0
4	390	110	1190	9	13	1230	255	15

<sup>a</sup>Time interval between radiant heating and aerodynamic heating.

TABLE III.- AERODYNAMIC FLOW CONDITIONS

Test	Free stream					Local				
	$T_t$ , K	$R$ , m <sup>-1</sup>	$M_\infty$	$q_\infty$ , kPa	$p_\infty$ , kPa	$M_1$	$q_1$ , kPa	$p_1$ , kPa	$\tau$ , Pa	$\delta^*$ , cm
1	1500	$5.22 \times 10^6$	6.13	54.5	2.10	6.13	54.5	2.10	58	1.3
2	1830	4.72	6.67	62.6	2.03	4.17	210	18	230	1.0
3	1780	4.99	6.61	64.0	2.12	6.61	64.0	2.12	53	1.3
4	1900	4.40	6.78	62.7	1.97	4.17	210	18	230	1.0



L-74-8413

Figure 1.- TPS panel installed in Langley 8-foot high-temperature structures tunnel.

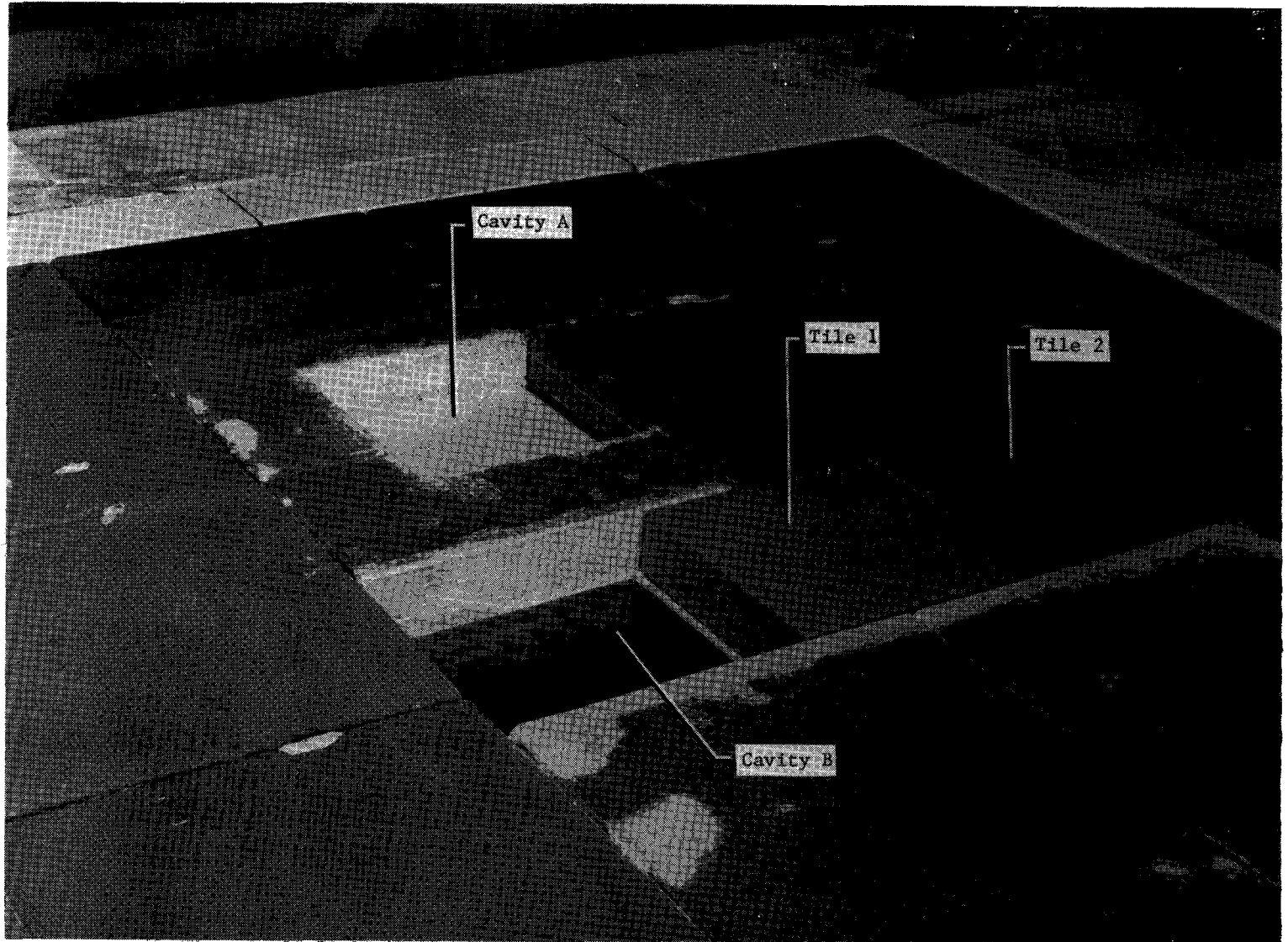


Figure 2.- Single lost-tile cavities.

L-75-1224.1

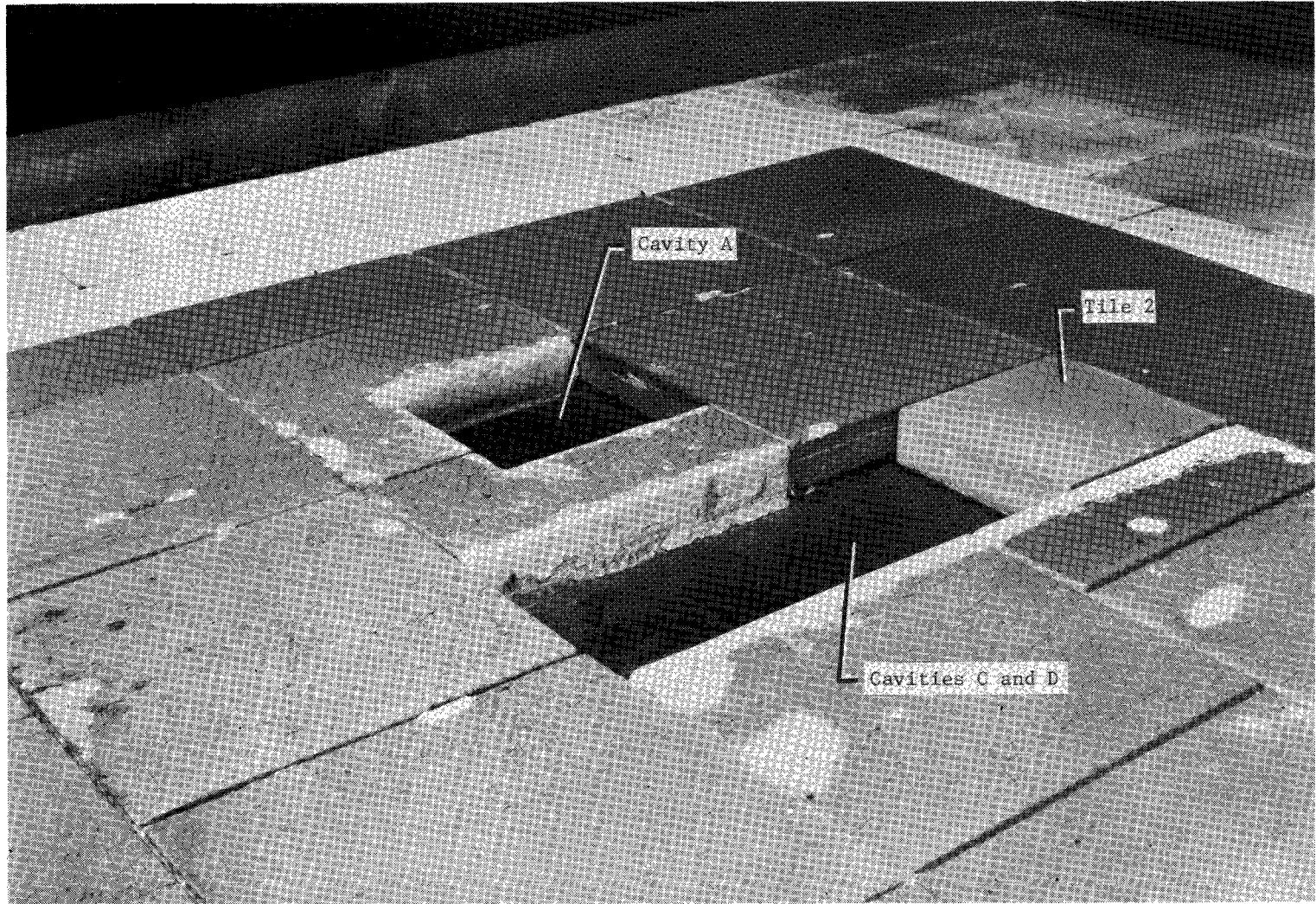
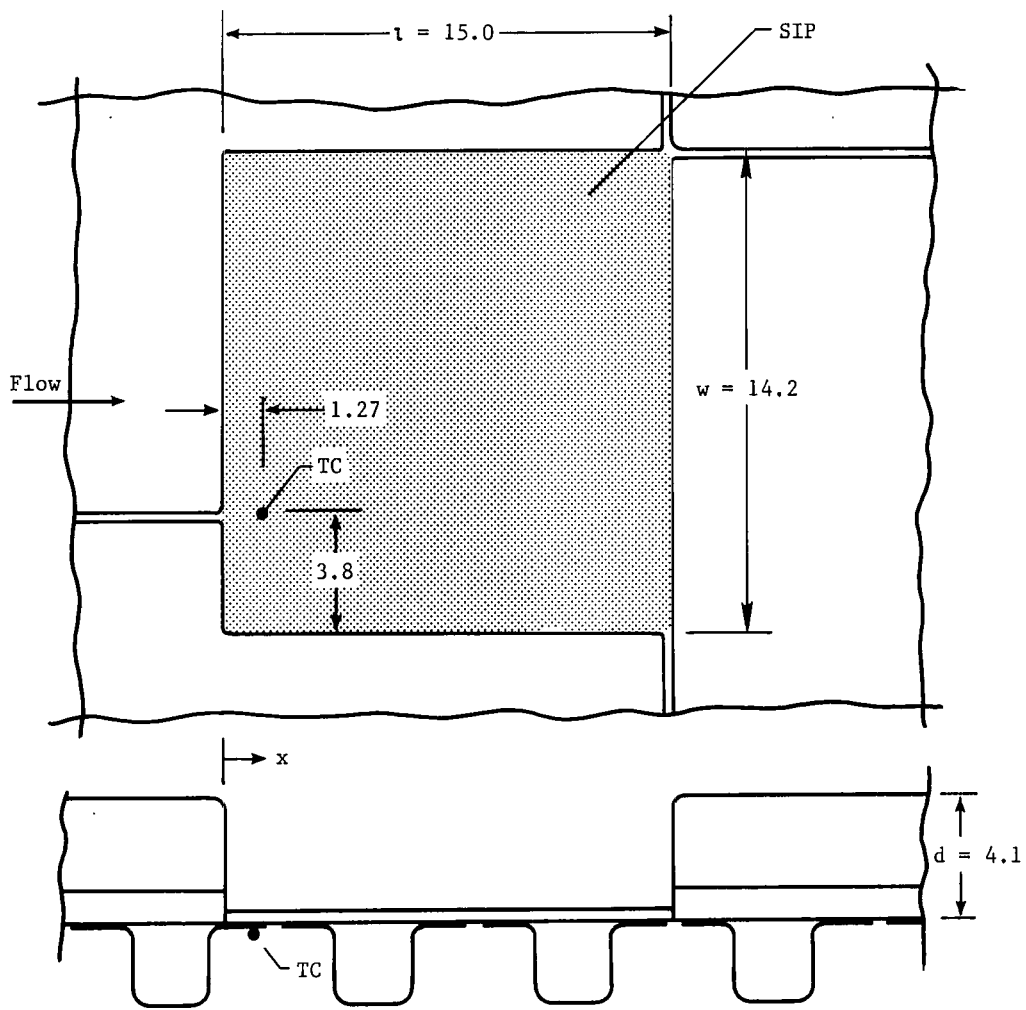


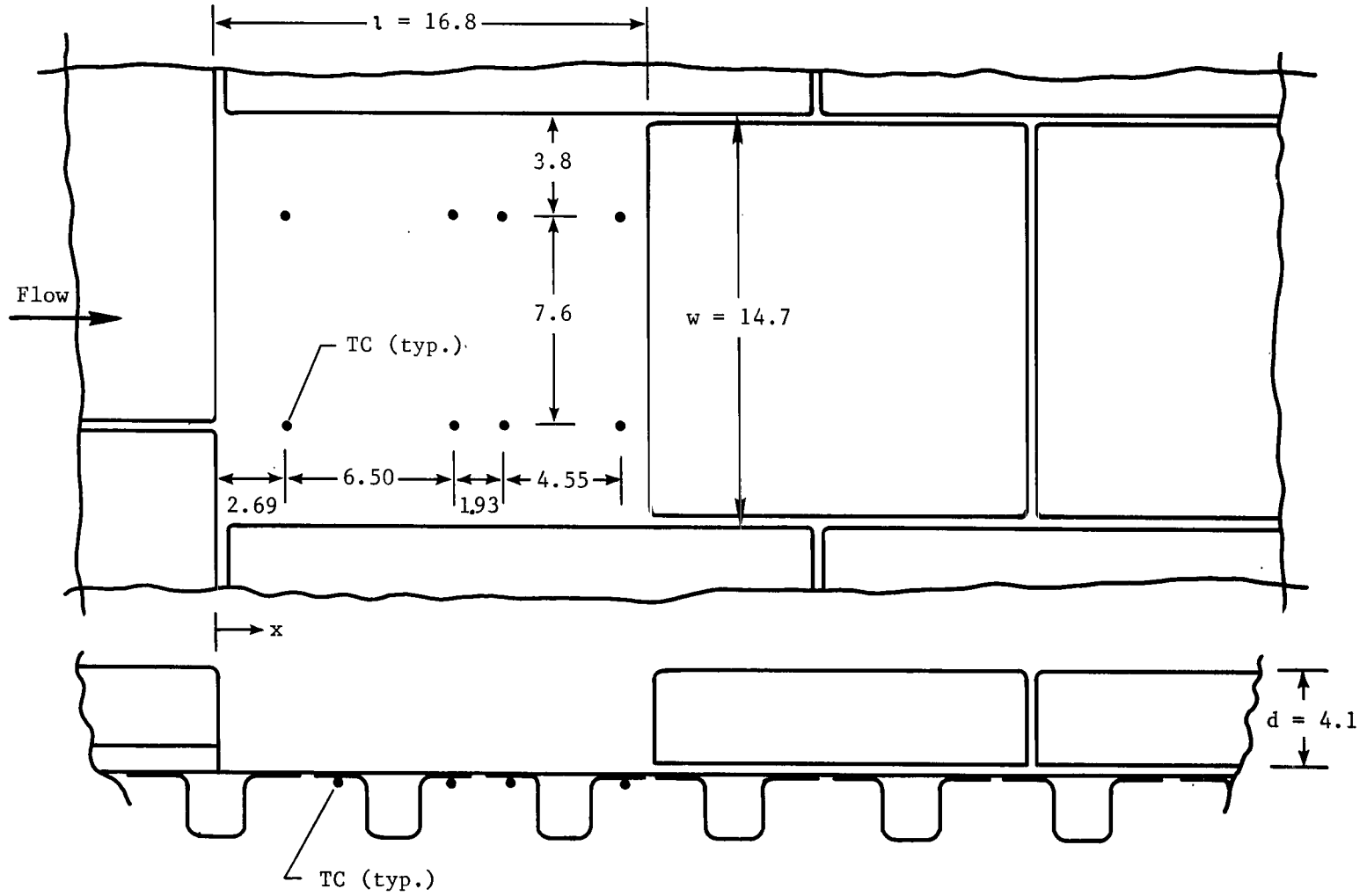
Figure 3.- Double lost-tile cavity.

L-75-1562.1



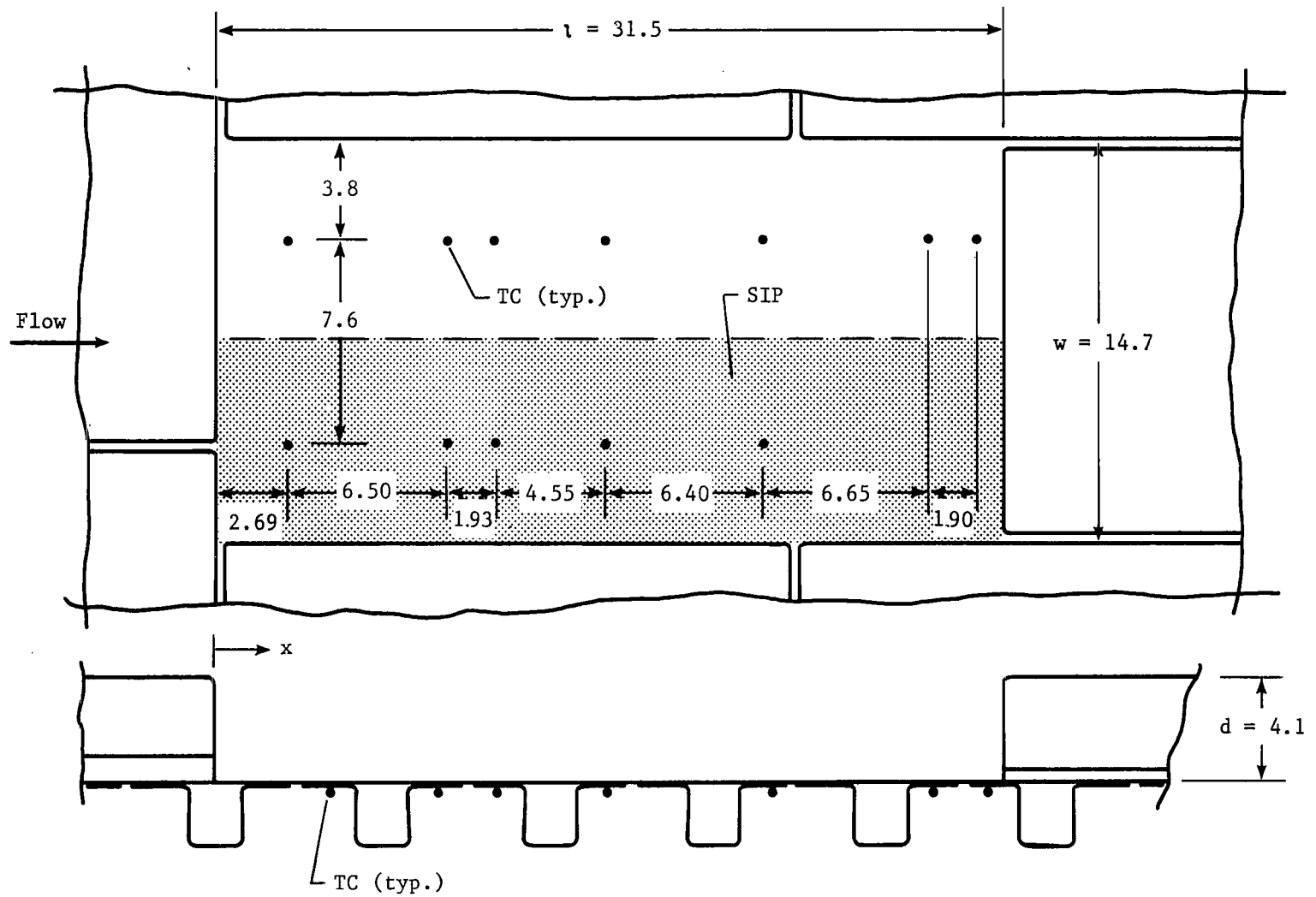
(a) Cavity A.

Figure 4.- Instrumentation details of lost-tile cavities. (All dimensions are in cm.)



(b) Cavity B.

Figure 4.- Continued.



(c) Cavities C and D.

Figure 4.- Concluded.

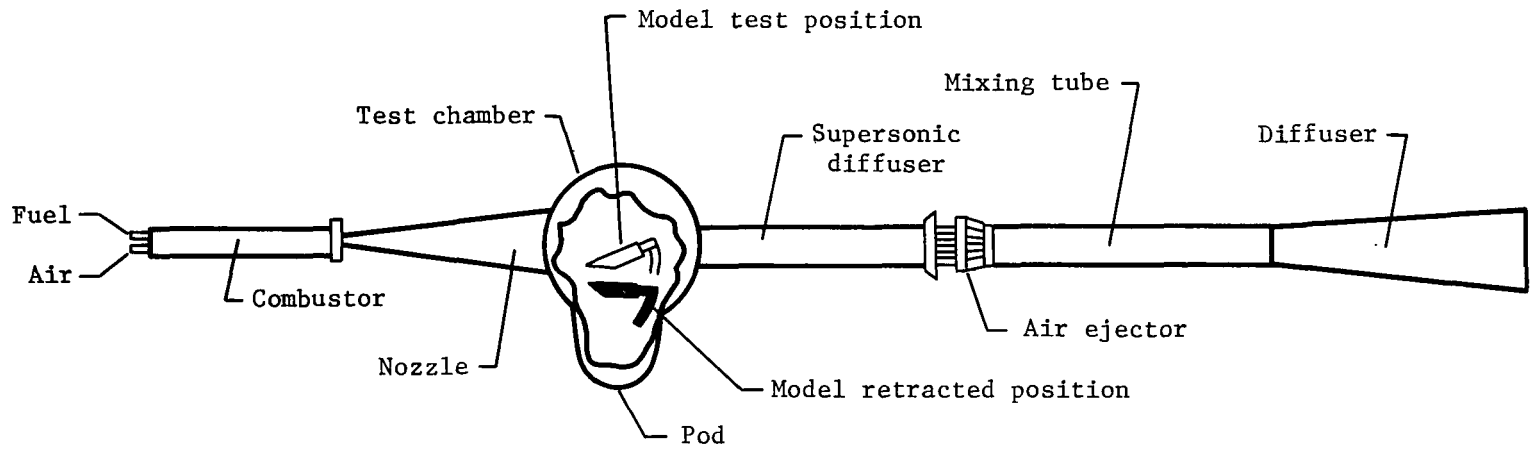
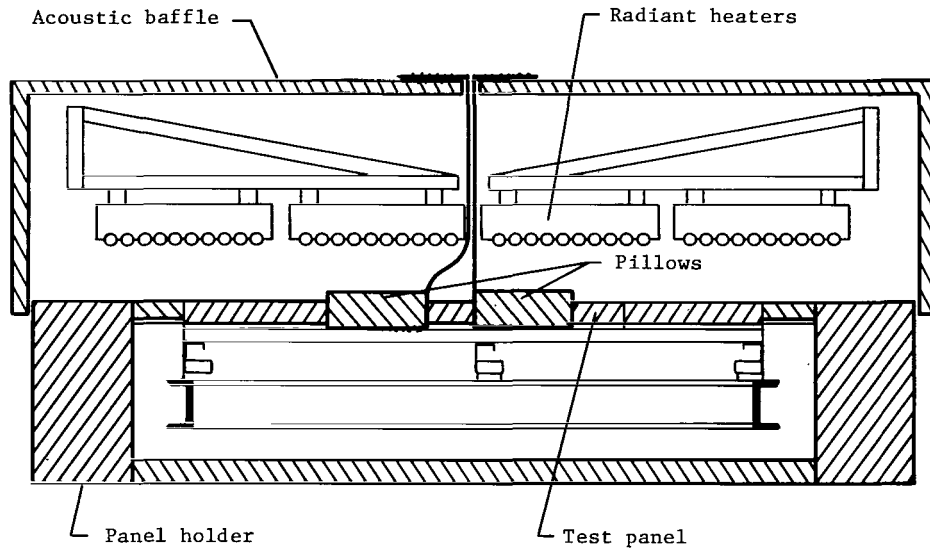
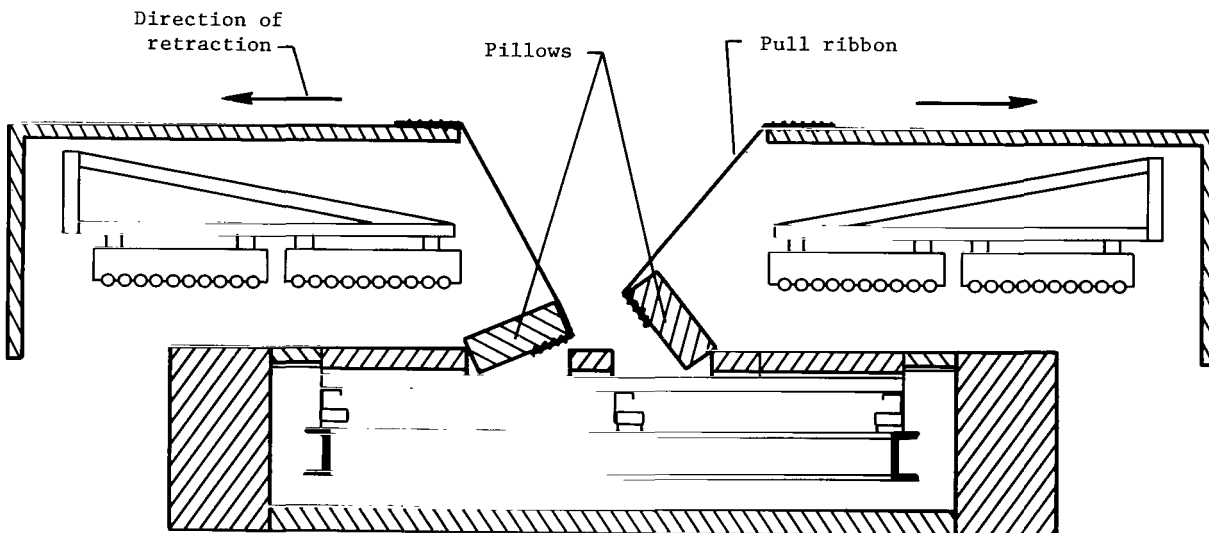


Figure 5.- Langley 8-foot high-temperature structures tunnel.





(a) Radiant heater position.



(b) Protective pillows extracted prior to model insertion into stream.

Figure 6.- Cross-sectional views illustrating method of uncovering test model.

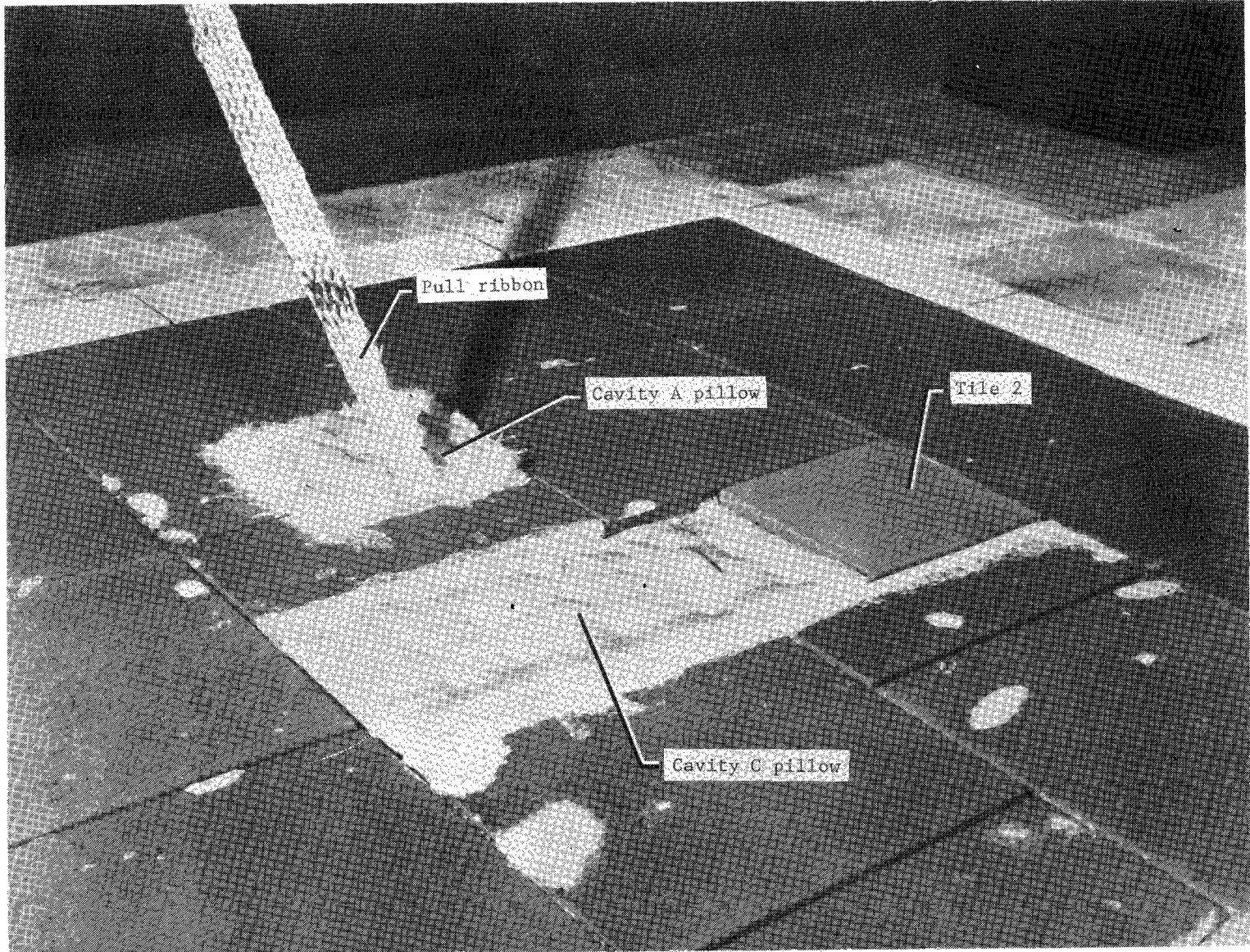
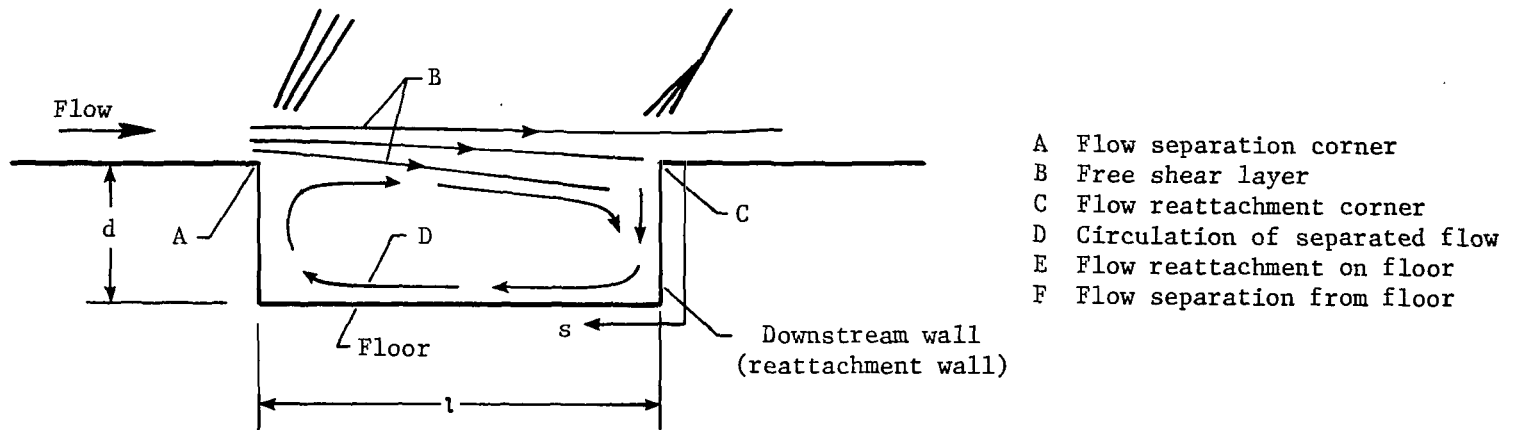
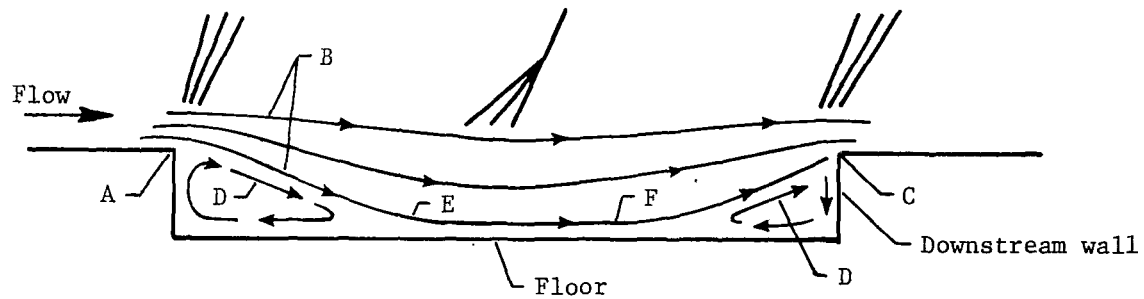


Figure 7.- Model with protective pillows in place.

L-75-1676.1

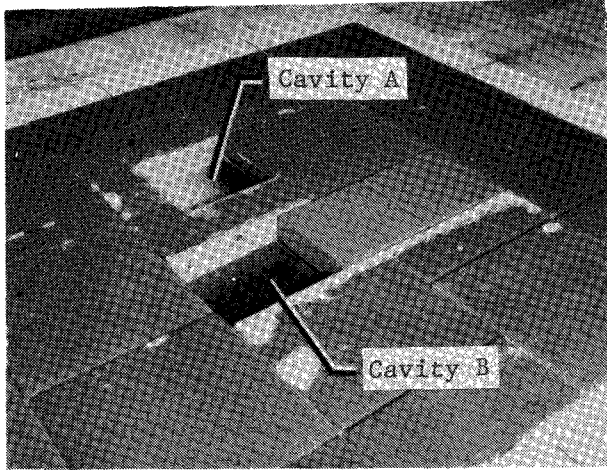


(a) Open cavity flow ( $l/d < 10$ ).

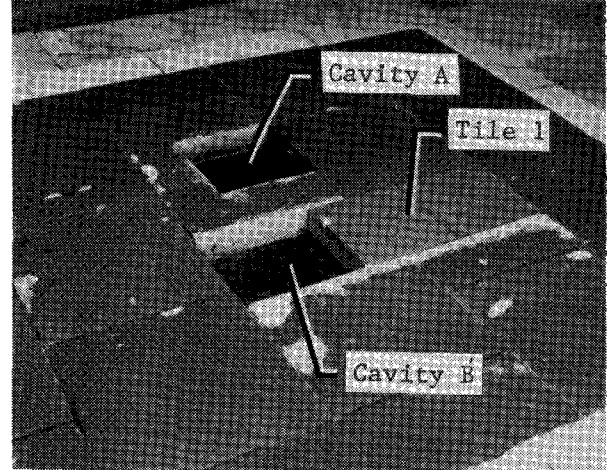


(b) Closed cavity flow ( $l/d > 14$ ).

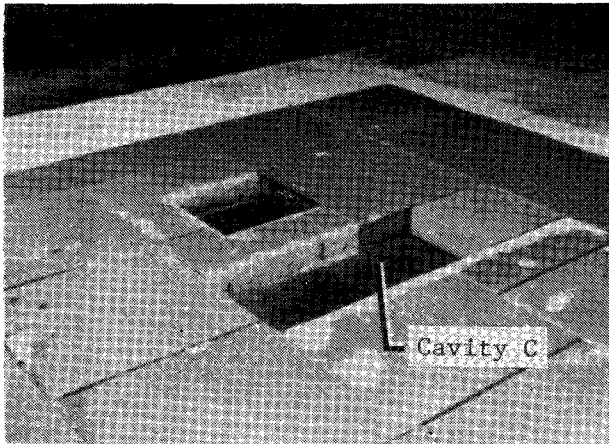
Figure 8.- Effect of cavity geometry on flow characteristics. (From ref. 4.)



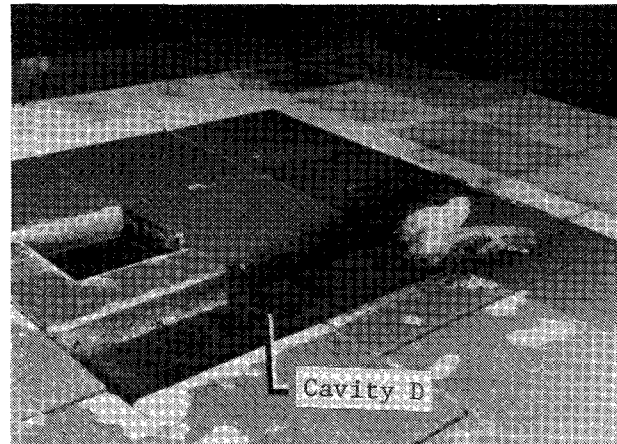
(a) Posttest 1.



(b) Posttest 2.



(c) Posttest 3.



(d) Posttest 4.

Figure 9.- Posttest condition of lost-tile cavities.

L-77-165

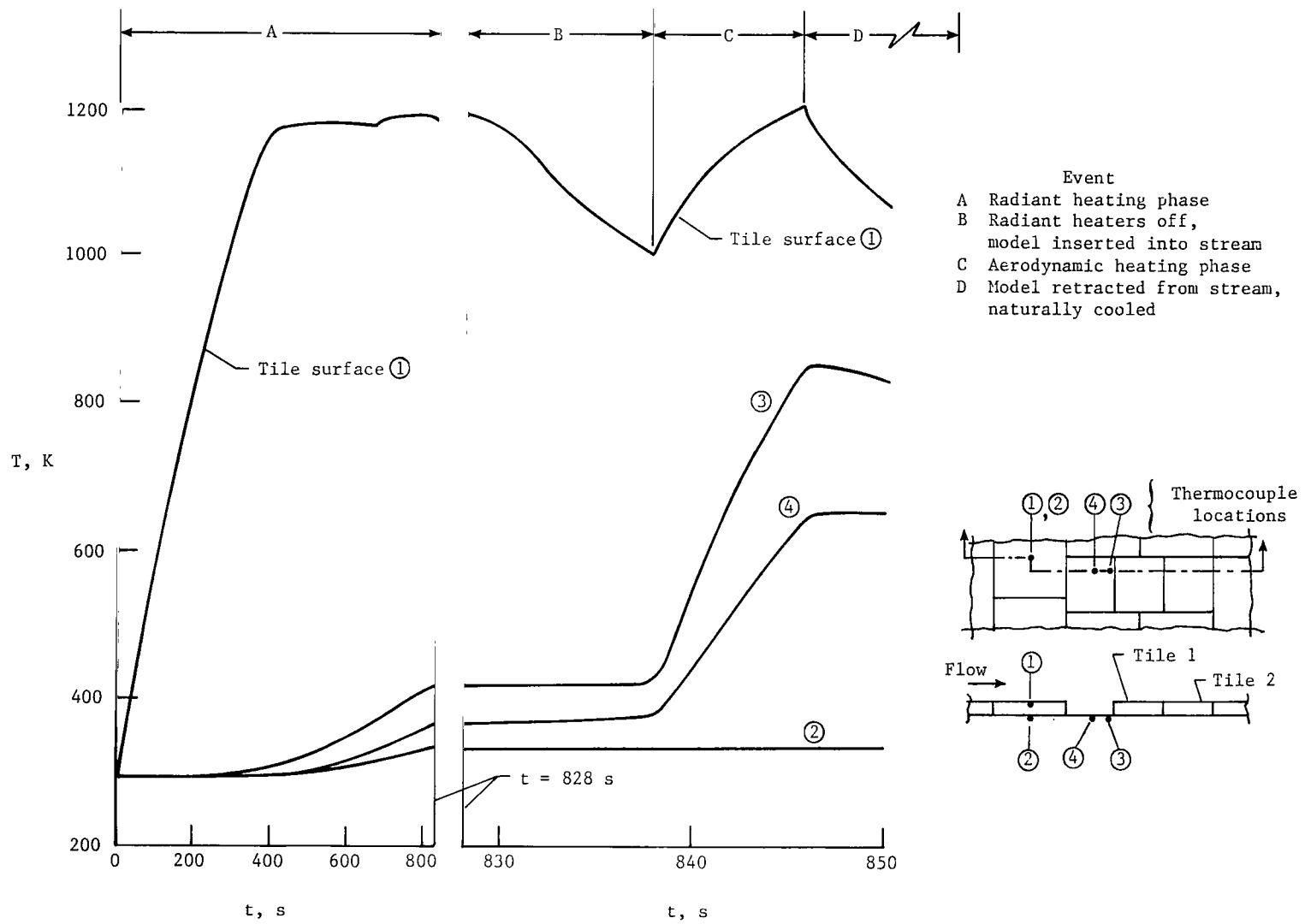
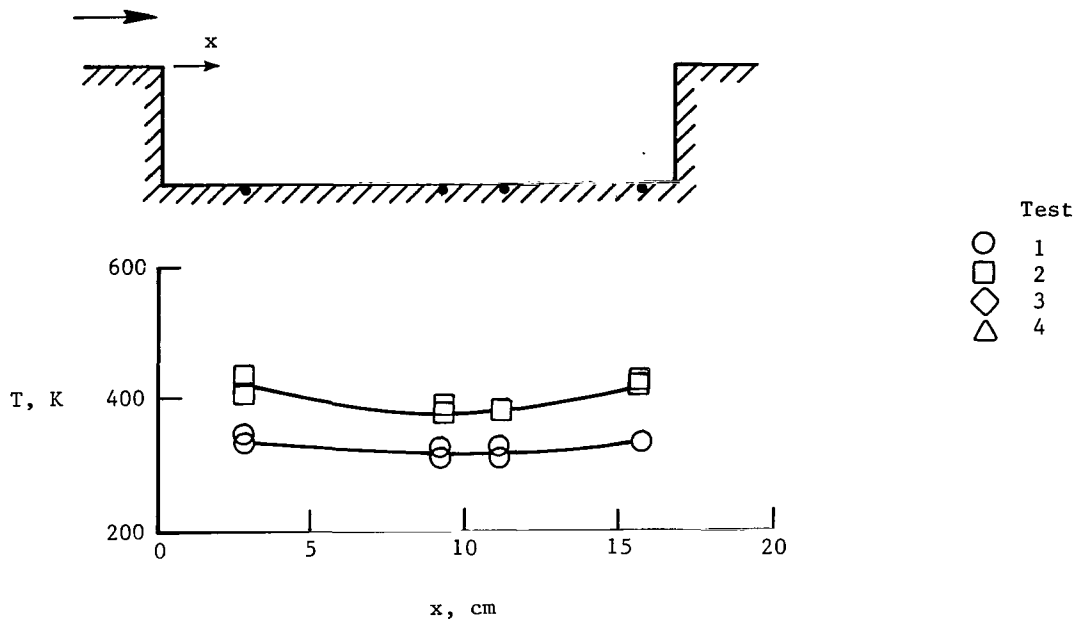
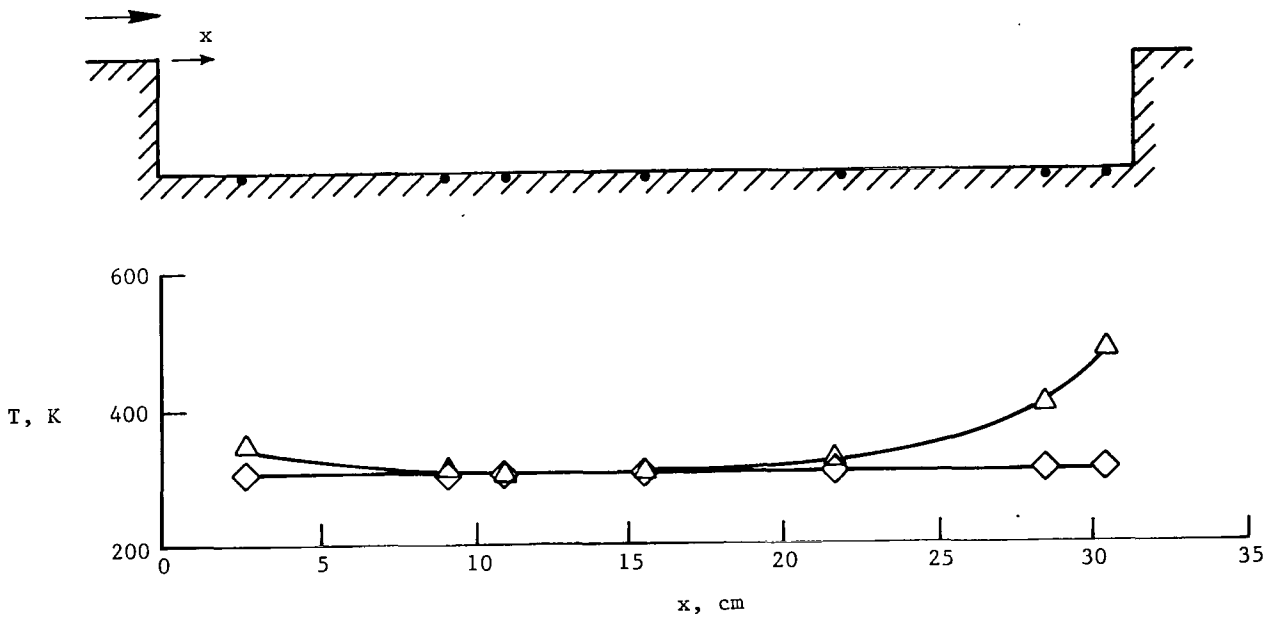


Figure 10.- Typical temperature histories of test 2.

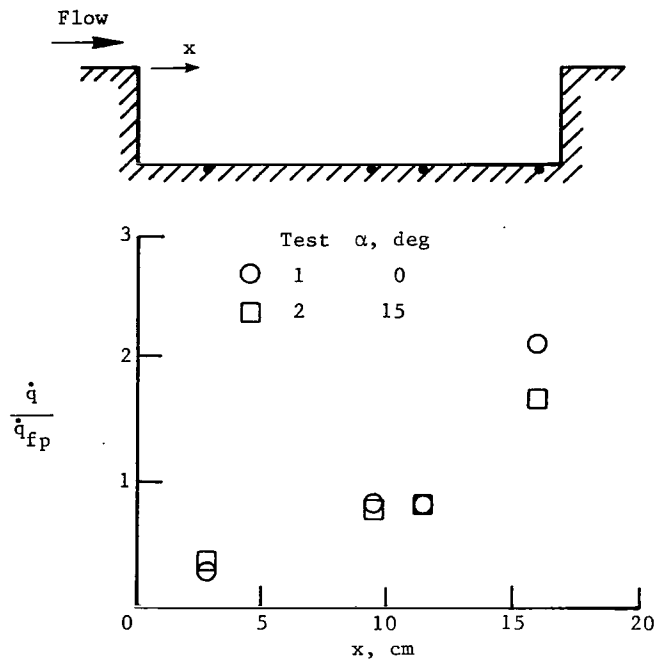


(a) Cavity B.

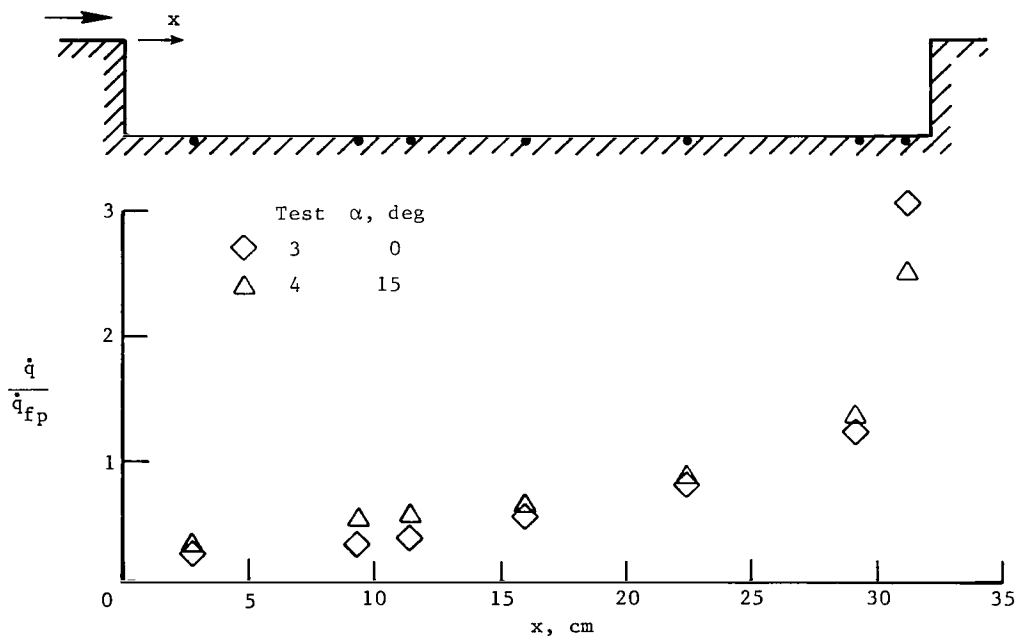


(b) Cavities C and D.

Figure 11.- Temperature distribution within lost-tile cavities after radiant heating phase.



(a) Single-tile cavity.



(b) Double-tile cavity.

Figure 12.- Heating-rate distributions on bare floor of lost-tile cavities.

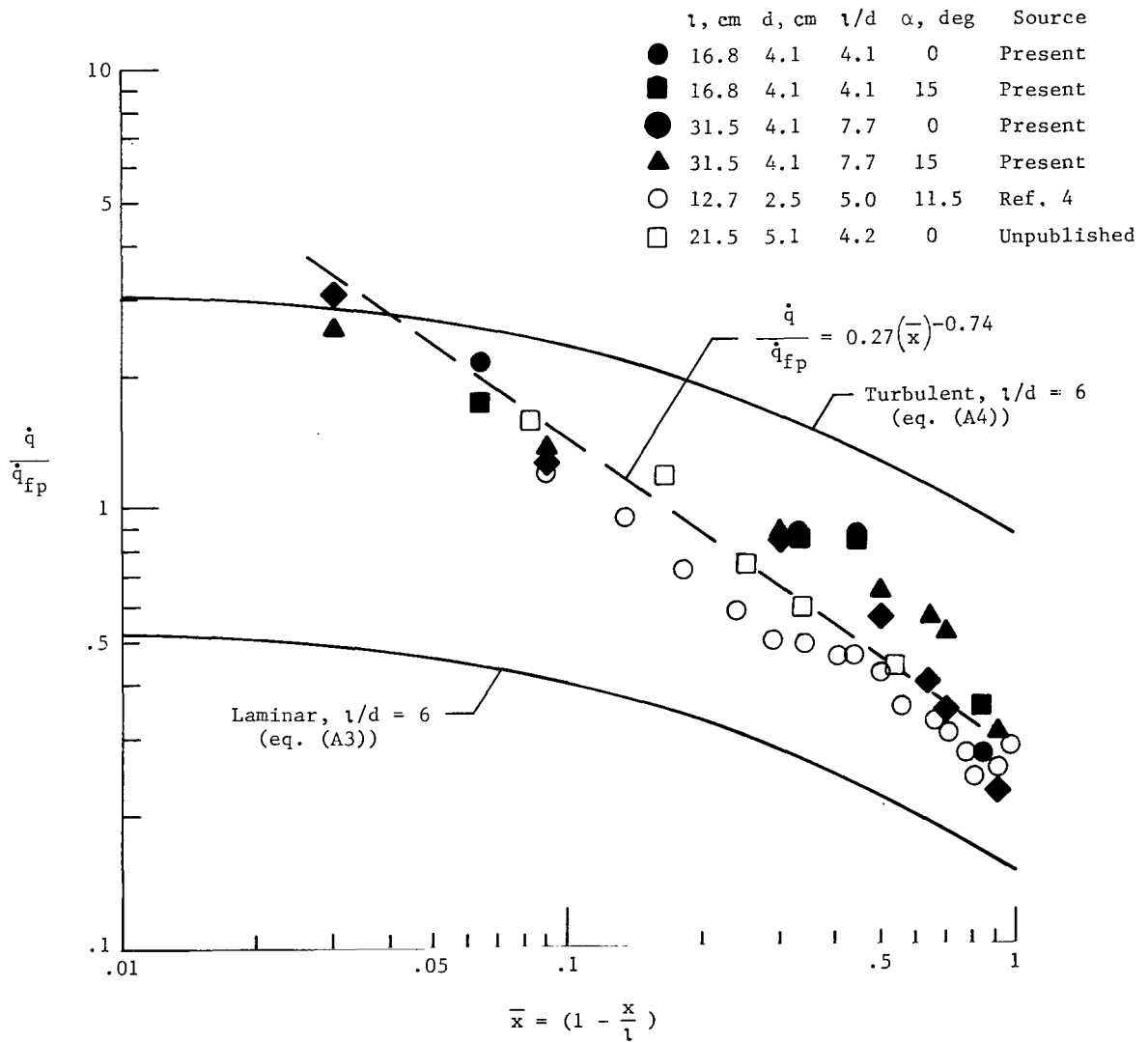
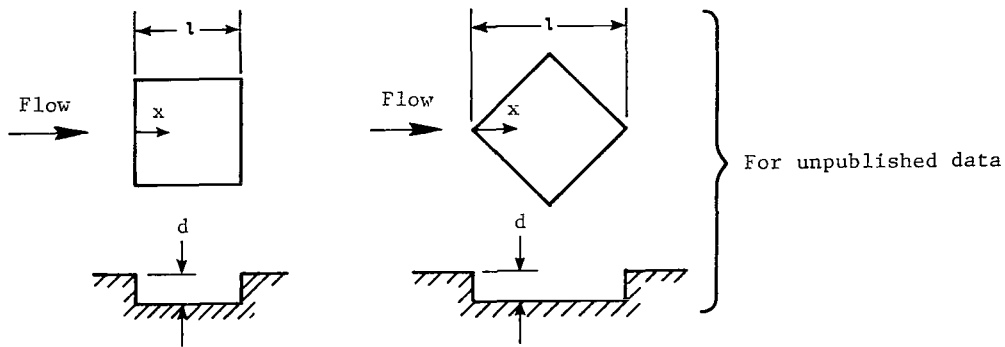
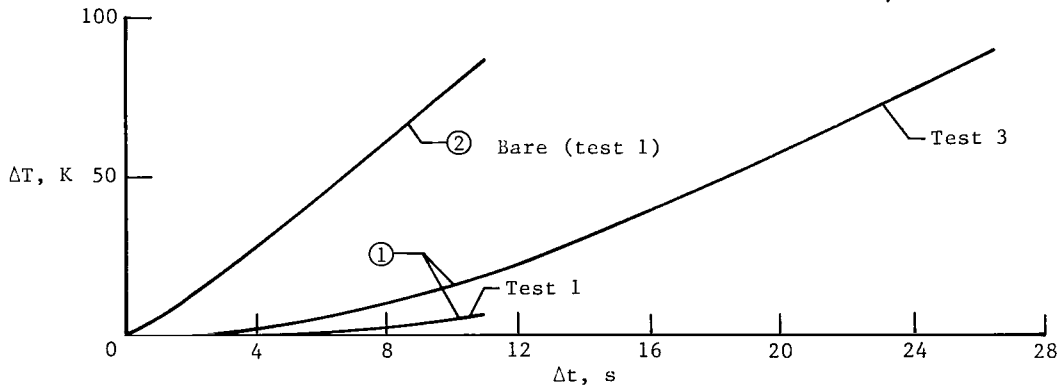
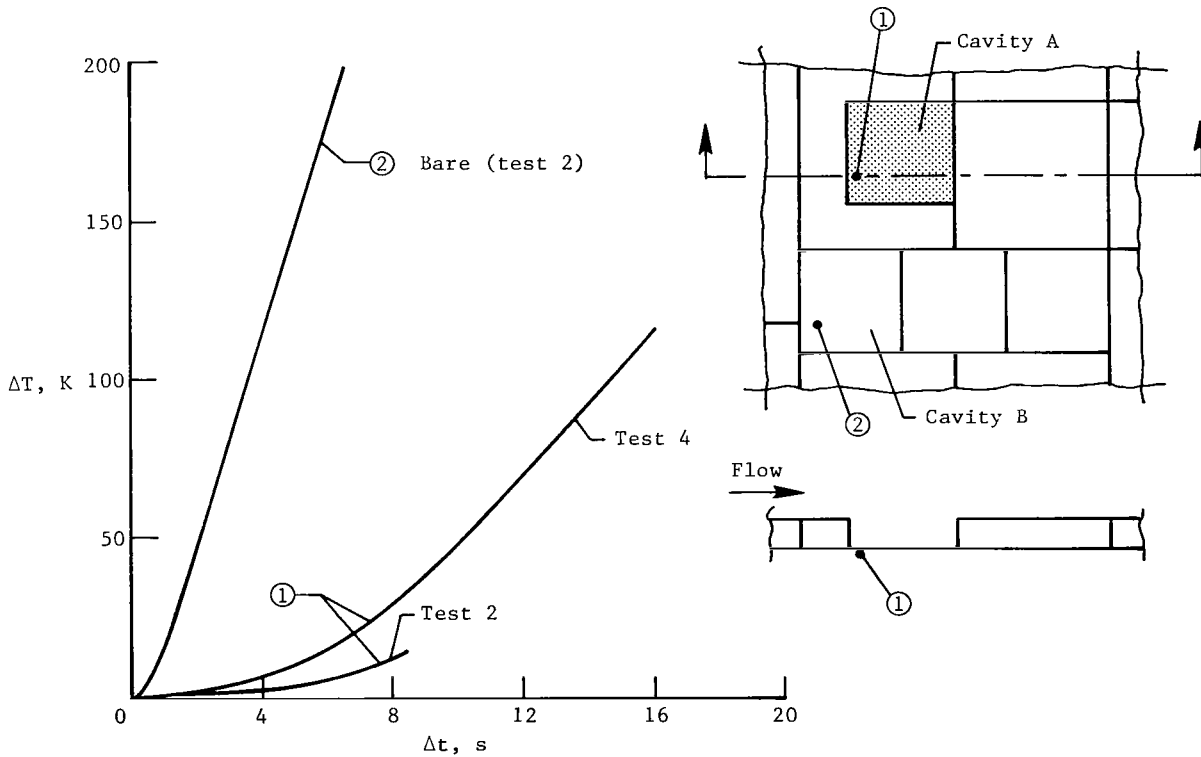


Figure 13.- Correlation of heating rate on floor of cavities.





(a)  $\alpha = 0^\circ$ .



(b)  $\alpha = 15^\circ$ .

Figure 14.- Temperature response of structure under single-tile cavity with and without SIP.

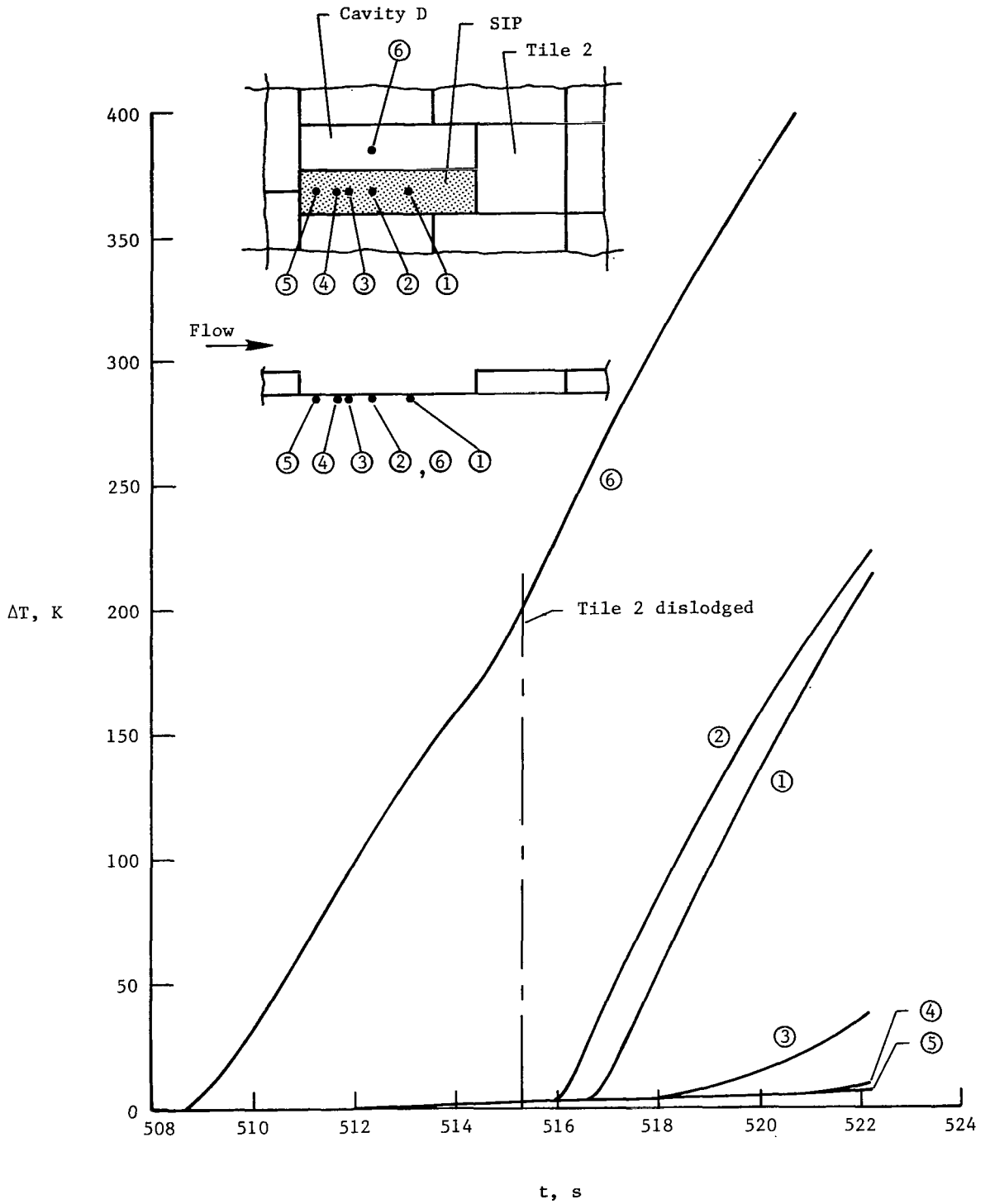
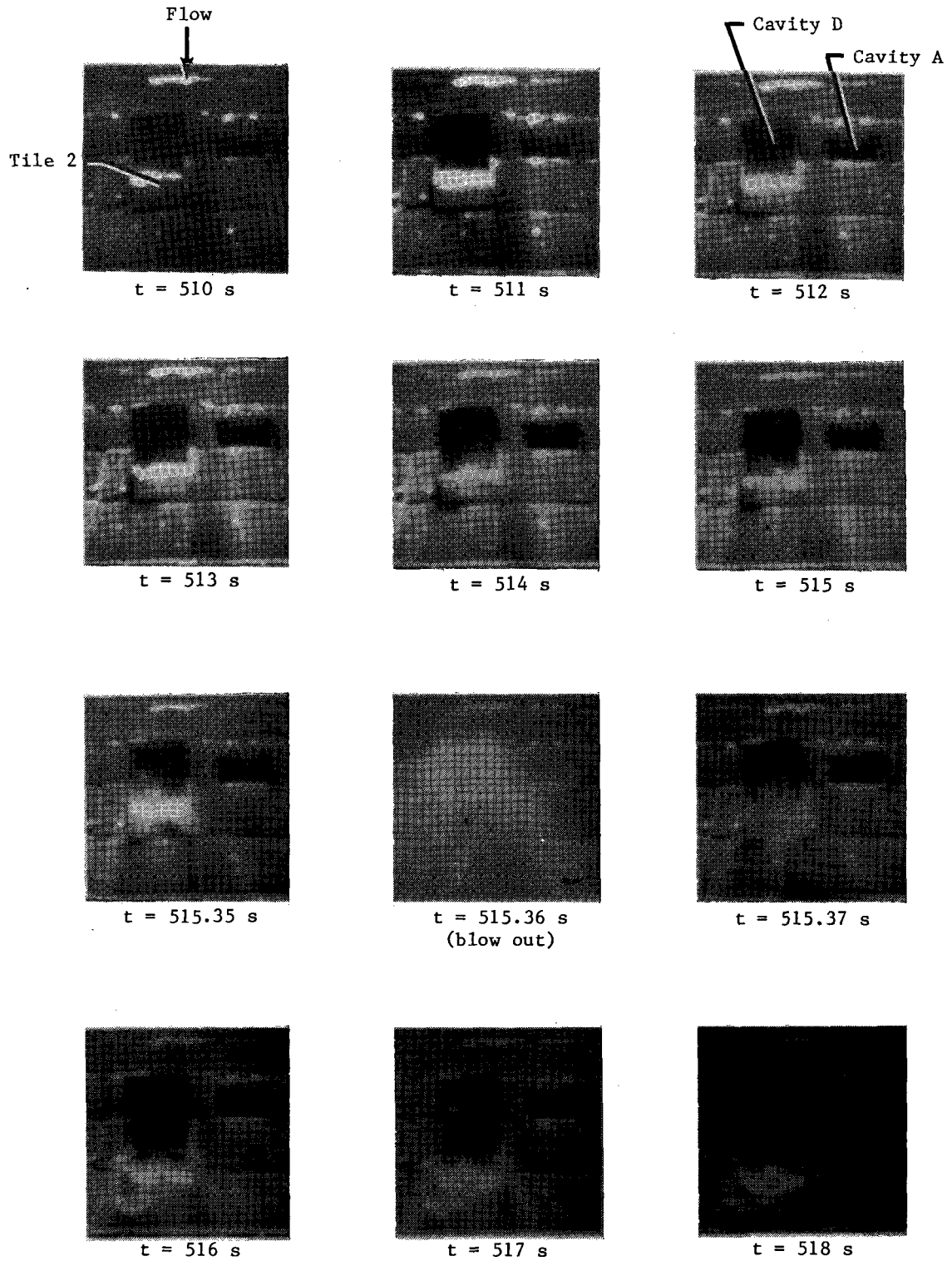


Figure 15.- Temperature response of structure under double-tile cavity with and without SIP (test 4).



L-77-166

Figure 16.- Photographic sequence of zippering failure.

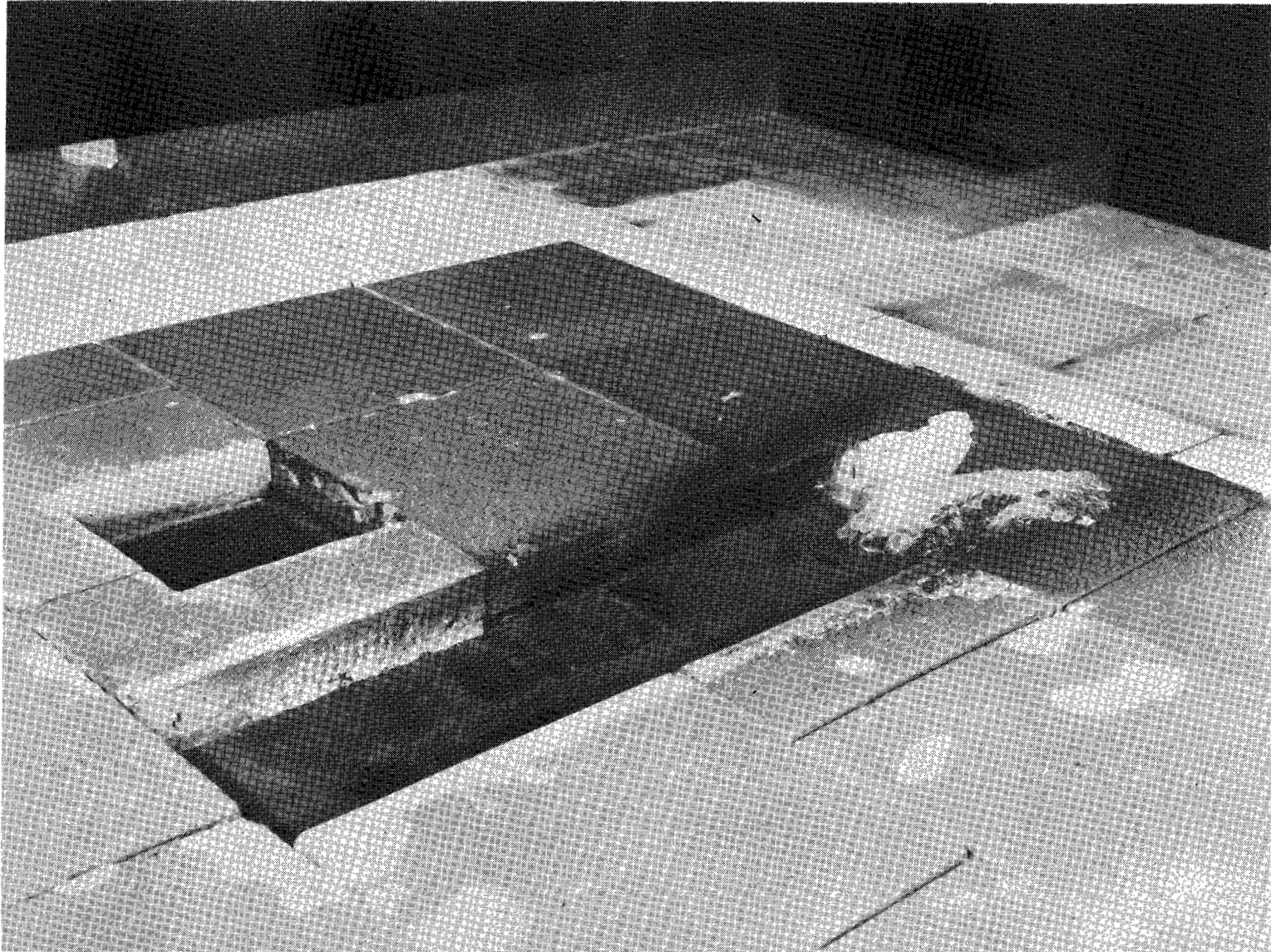


Figure 17.- Cavity D after test 4.

L-75-1705

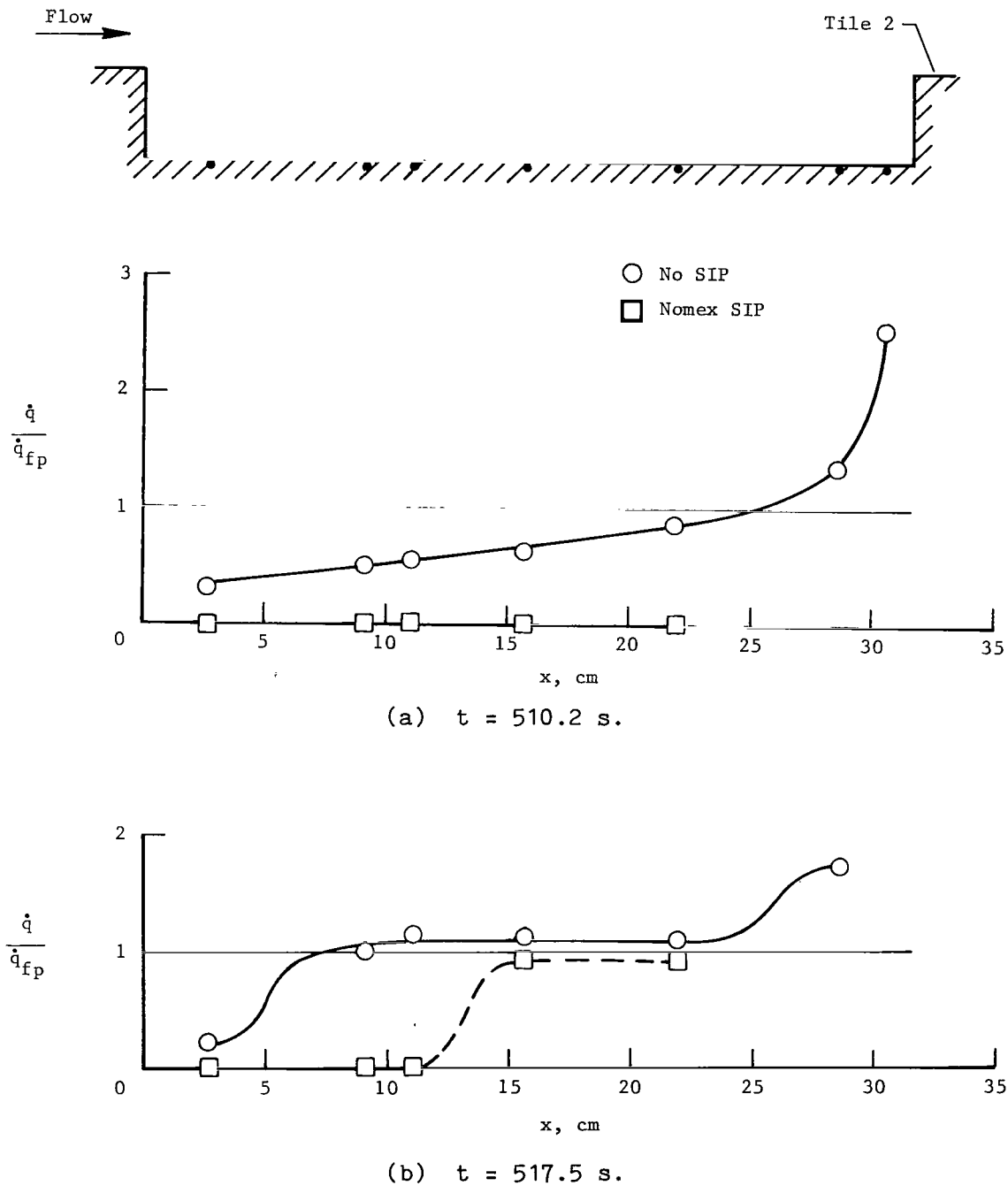


Figure 18.- Aerodynamic heating-rate distribution within cavity D before and after tile 2 blew out.

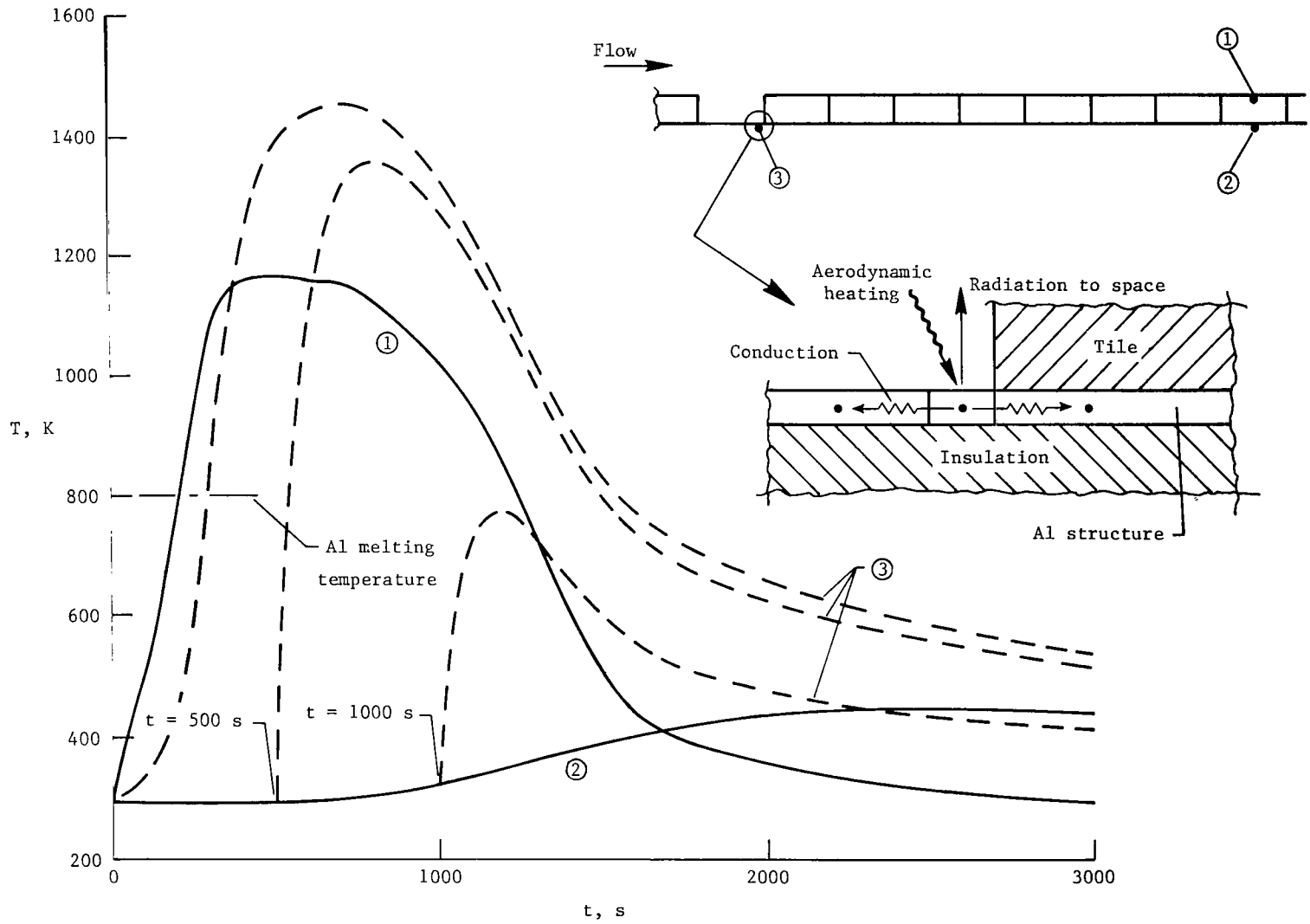


Figure 19. Calculated thermal response of primary structure in lost-tile cavity exposed to shuttle entry.



258 001 C1 U D 770401 S00903DS  
DEPT OF THE AIR FORCE  
AF WEAPONS LABORATORY  
ATTN: TECHNICAL LIBRARY (SUL)  
KIRTLAND AFB NM 87117

POSTMASTER: If Undeliverable (Section 158  
Postal Manual) Do Not Return

*"The aeronautical and space activities of the United States shall be conducted so as to contribute . . . to the expansion of human knowledge of phenomena in the atmosphere and space. The Administration shall provide for the widest practicable and appropriate dissemination of information concerning its activities and the results thereof."*

—NATIONAL AERONAUTICS AND SPACE ACT OF 1958

## NASA SCIENTIFIC AND TECHNICAL PUBLICATIONS

**TECHNICAL REPORTS:** Scientific and technical information considered important, complete, and a lasting contribution to existing knowledge.

**TECHNICAL NOTES:** Information less broad in scope but nevertheless of importance as a contribution to existing knowledge.

**TECHNICAL MEMORANDUMS:** Information receiving limited distribution because of preliminary data, security classification, or other reasons. Also includes conference proceedings with either limited or unlimited distribution.

**CONTRACTOR REPORTS:** Scientific and technical information generated under a NASA contract or grant and considered an important contribution to existing knowledge.

**TECHNICAL TRANSLATIONS:** Information published in a foreign language considered to merit NASA distribution in English.

**SPECIAL PUBLICATIONS:** Information derived from or of value to NASA activities. Publications include final reports of major projects, monographs, data compilations, handbooks, sourcebooks, and special bibliographies.

**TECHNOLOGY UTILIZATION PUBLICATIONS:** Information on technology used by NASA that may be of particular interest in commercial and other non-aerospace applications. Publications include Tech Briefs, Technology Utilization Reports and Technology Surveys.

*Details on the availability of these publications may be obtained from:*

**SCIENTIFIC AND TECHNICAL INFORMATION OFFICE**

**NATIONAL AERONAUTICS AND SPACE ADMINISTRATION**  
Washington, D.C. 20546